3224 *Inorg. Chem.* **2010**, *49*, 3224–3238
DOI: 10.1021/ic9020756

Inorganic Chemistry
Article

# $Mn^{2+}$ Complexes with Pyridine-Containing 15-Membered Macrocycles: Thermodynamic, Kinetic, Crystallographic, and $^1H/^{17}O$ Relaxation Studies

**Bohuslav Drahoš,[†,‡] Jan Kotek,[†] Petr Hermann,[†] Ivan Lukeš,[*,†] and Éva Tóth[*,‡]**

[†]*Department of Inorganic Chemistry, Faculty of Science, Universita Karlova (Charles University), Hlavova 2030, 128 43 Prague 2, Czech Republic, and* [‡]*Centre de Biophysique Moléculaire, CNRS, rue Charles Sadron, 45071 Orléans, France*

Received October 21, 2009

Given its five unpaired d-electrons, long electronic relaxation time, and fast water exchange, $Mn^{2+}$ is a potential candidate for contrast agent application in medical magnetic resonance imaging. Nevertheless, the design of chelators that ensure stable $Mn^{2+}$ complexation and optimal relaxation properties remains a coordination chemistry challenge. Here, we report the synthesis of two pyridine-containing ligands **L1** and **L2**, with 15-membered triaza-dioxa-crown and pentaaza-crown ether macrocycles, respectively, and the characterization of their $Mn^{2+}$ complexes. Protonation constants of the ligands and stability constants of various metal complexes were determined by potentiometry. The presence of the pyridine in the macrocyclic ring induces rigidity of the complexes which results in a greater thermodynamic stability with respect to the nonpyridine analogues. Solid-state structures of Mn**L1** and Mn**L2** confirmed seven-coordination of $Mn^{2+}$ with $Cl^-$ and $H_2O$ in axial positions. The dissociation kinetics of Mn**L2** in the presence of $Zn^{2+}$ were followed by relaxometric measurements. They proved the prime importance of the proton-assisted dissociation while the zinc(II)-assisted pathway is not important at physiological pH. For Mn**L1**, the dissociation was too fast to be studied by conventional relaxivity measurements under pH 6. A combined $^{17}O$ NMR and $^1H$ NMRD study on Mn**L1** and Mn**L2** yielded the parameters that govern the relaxivity of these complexes. The water exchange rate for Mn**L1**, $k_{ex}^{298} = 0.38 \times 10^7\ s^{-1}$, is the lowest value ever reported for a $Mn^{2+}$ complex, while a considerably higher value was obtained for Mn**L2** ($k_{ex}^{298} = 6.9 \times 10^7\ s^{-1}$). Anion binding was studied by relaxometric titrations. They revealed weak interactions between Mn**L2** and phosphate or citrate, leading to the formation of monohydrated species. Overall, the incorporation of a pyridine into a polyaza macrocycle scaffold has several beneficial effects on the $Mn^{2+}$ chelates with respect to potential MRI contrast agent applications: (*i*) The thermodynamic and the kinetic stability of the complexes is increased. (*ii*) The rigidified ligand backbone results in higher coordination numbers of the metal ion, allowing for two inner-sphere water molecules in aqueous solution.

## Introduction

Today, magnetic resonance imaging (MRI) is one of the most powerful diagnostic methods in clinical medicine. The intrinsically low sensitivity of MRI is often improved by the application of contrast agents (CA); about 40% of all MRI examinations are made after administration of a contrast medium. These paramagnetic substances reduce the longitudinal ($T_1$) and transverse ($T_2$) relaxation times of water protons in the body tissue resulting in an increased image contrast. Nowadays, the majority of contrast agents used in the clinics are $Gd^{3+}$ complexes that affect primarily the $T_1$ relaxation time of water protons and provide positive contrast on $T_1$-weighted MR images.[1−3]

The efficiency of a CA is described by its proton relaxivity ($r_1$) which is defined as the paramagnetic enhancement of the longitudinal water proton relaxation rate referred to 1 mM concentration of the agent. The overall relaxivity is determined by microscopic properties of the paramagnetic complex and originates from inner- and outer-sphere mechanisms.[1] The inner-sphere relaxivity contribution is due to the presence of water molecule(s) in the first coordination sphere of the paramagnetic ion that exchange with the surrounding water, thus transmitting the paramagnetic effect of the metal ion to the bulk. Consequently, the inner-sphere relaxivity is linearly proportional to the number of coordinated water molecules (hydration number, $q$) and also depends on their exchange rate, $k_{ex}$. The rotational motion of the chelate, described by the rotational correlation time, $\tau_r$, as well as the

*To whom correspondence should be addressed. Tel.: +33 2 38 25 76 25 (É.T.); +420 2 2195 1259 (I.L.). Fax: +33 2 38 63 15 17 (É.T.); +420 2 2195 1253 (I.L.). E-mail: eva.jakabtoth@cnrs-orleans.fr (É.T.); lukes@natur.cuni.cz (I.L.).

(1) *The Chemistry of Contrast Agents in Medical Magnetic Resonance Imaging*; Tóth, É., Merbach, A. E., Eds.; John Wiley & Sons: Chichester, 2001.

(2) Caravan, P.; Ellison, J. J.; McMurry, T. J.; Lauffer, R. B. *Chem. Rev.* **1999**, *99*, 2293–2352.

(3) Hermann, P.; Kotek, J.; Kubíček, V.; Lukeš, I. *Dalton Trans.* **2008**, 3027–3047.


Published on Web 02/24/2010

**Chart 1.** Structures of the Ligands Studied or Discussed in the Text

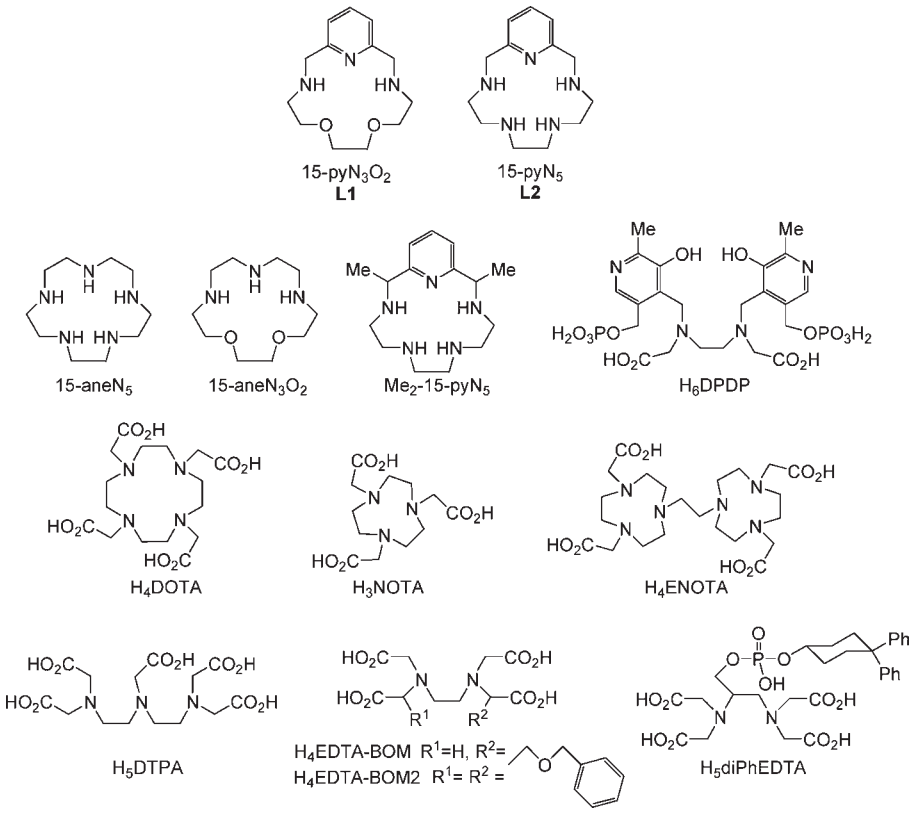


relaxation rates of the electron spin of the metal ion, $T_{1,2e}$, are other important parameters determining relaxivity. The outer-sphere relaxivity term arises from the random translation diffusion of water protons in the proximity of the paramagnetic ion and contributes up to 50% to the overall relaxivity for small-molecular-weight chelates.

While $Gd^{3+}$ complexes have been extensively studied in the context of MRI, much less attention has been devoted to paramagnetic transition metals. Among them, $Mn^{2+}$ is the best candidate given its high spin (5 unpaired electrons) and slow electronic relaxation. One advantage of $Mn^{2+}$ complexes could be their fast water exchange, which is often in the optimal range to attain high relaxivities, while this factor can be highly limitative for $Gd^{3+}$-based agents.

Manganese is a biogenic element. It is a cofactor in several enzymes such as manganese superoxide dismutase[4] or glutamine synthetase.[5] Due to their similar ionic radius, $Mn^{2+}$ shows biological and chemical similarity to $Ca^{2+}$, enabling, e.g., calcium influx detection,[6] and has a high affinity for $Ca^{2+}$ and $Mg^{2+}$ binding sites in proteins[7] and nucleic acids.[8] The free $Mn^{2+}$ aqua ion shows toxicity only at higher concentrations.[9] Nevertheless, the accumulation of $Mn^{2+}$ has been proven in the brain,[10] which can lead to neurological disorders resembling Parkinson's disease.[11]

In the current medical practice, only one $Mn^{2+}$-based CA, $[Mn(DPDP)]^{4-}$, is used in liver or cardiac imaging ($DPDP^{6-}$ = *N*,*N*′-dipyridoxylethylenediamine-*N*,*N*′-diacetate-5,5′-bis-(phosphate); Chart 1).[12,13] The complex itself has no coordinated water molecule, and the observed *in vivo* relaxation effect comes from free $Mn^{2+}$ released from the chelate. The presence of the ligand is only important to ensure a slow release of $Mn^{2+}$ which prevents toxicity observed on the direct application of simple manganese(II) salts. Indeed, a specific field of application of $Mn^{2+}$ in MRI is manganese enhanced magnetic resonance imaging (MEMRI), where mostly manganese(II) chloride is used.[14] The main drawback of this method is manganese toxicity for concentrations providing sufficient contrast; thus, MEMRI is limited to small animal imaging. The design of ligands simultaneously satisfying stable $Mn^{2+}$ complexation and good MRI efficiency remains a coordination chemistry challenge.[15] Indeed, the high complex stability and the presence of water molecule(s) directly coordinated to $Mn^{2+}$ are often contradictory requirements. Consequently, relatively few data have been reported on $Mn^{2+}$ chelates in the context of MRI contrast agent applications. The $Mn^{2+}$ complexes studied so far involve chelates of

(4) Li, Y.; Huang, T. T.; Carlson, E. J.; Melov, S.; Ursell, P. C.; Olson, J. L.; Noble, L. J.; Yoshimura, M. P.; Berger, C.; Chan, P. H. *Nat. Genet.* **1995**, *11*, 376–381.
(5) Wedler, F. C.; Denman, R. B. *Curr. Top. Cell Regul.* **1984**, *24*, 153–169.
(6) Aoki, I.; Naruse, S.; Takana, C. *NMR Biomed.* **2004**, *17*, 569–580.
(7) Mildvan, A. S.; Cohn, M. *Biochemistry* **1963**, *338*, 910–919.
(8) Eisinger, J.; Fawaz-Estrup, F.; Shulman, R. G. *J. Chem. Phys.* **1965**, *42*, 43–53.
(9) (a) Kang, Y. S.; Gore, J. C. *Invest. Radiol.* **1984**, *19*, 399–407. (b) Crossgrove, J.; Zheng, W. *NMR Biomed.* **2004**, *17*, 544–553.
(10) Lucchini, R.; Albini, E.; Placidi, D.; Gasparotti, R.; Pigozzi, M. G.; Montani, G.; Alessio, L. *Neurotoxicology* **2000**, *21*, 769–775.
(11) Olanow, C. W. *Ann. N.Y. Acad. Sci.* **2004**, *1012*, 209–223.
(12) Rocklage, S. M.; Cacheris, W. P.; Quay, S. C.; Hahn, F. E.; Raymond, K. N. *Inorg. Chem.* **1989**, *28*, 477–485.
(13) Murakami, T.; Baron, R. L.; Peterson, M. S.; Oliver, J. H., III; Davis, P. L.; Confer, B. S.; Federle, M. P. *Radiology* **1996**, *200*, 69–77.
(14) *NMR Biomed.* **2004**, *17*, 527−634. Issue No. 8 is dedicated to the Manganese Enhanced Magnetic Resonance Imaging (MEMRI).
(15) Caravan, P.; Farrar, C. T.; Frullano, L.; Uppal, R. *Contrast Media Mol. Imaging* **2009**, *4*, 89–100.

linear polydentate ligands, like $EDTA^{4-}$[16–19] or $DTPA^{5-}$ derivatives,[20] or of macrocycle-based ligands, $NOTA^{3-}$[21,22] and $DOTA^{4-}$ (Chart 1).[18,21,23,24] These complexes have a maximum of one water molecule in the first coordination sphere. Creating ligands that form bishydrated $Mn^{2+}$ complexes of sufficient stability is a considerable problem and likely needs macrocyclic structures.

Due to the lack of crystal-field stabilization caused by the $d^5$ electron configuration of $Mn^{2+}$ and a lower positive charge, $Mn^{2+}$ complexes are, in general, thermodynamically less stable than their transition metal ion or $Gd^{3+}$ analogues. Therefore, their kinetic stability can play a very important role in preventing *in vivo* toxicity. So far, dissociation or transmetalation kinetic data for $Mn^{2+}$ chelates has not been reported in the literature.

With the objective of exploring novel ligand systems that simultaneously ensure stable $Mn^{2+}$ complexation and high efficiency in potential MRI applications, we have considered 15-membered aza-crown ethers. Such systems have been extensively investigated as superoxide dismutase (SOD) mimics.[25,26] We have synthesized pyridine-derivative macrocycles **L1** and **L2** (Chart 1) and investigated their $Mn^{2+}$ complexes. These ligands are expected to provide a structural motif ensuring balance between complex stability, the presence of coordinated water, and suitable microscopic parameters governing relaxivity. The introduction of a pyridine ring into the macrocycle skeleton will rigidify the complex, which can contribute to an increased kinetic stability, as it has been observed for linear[27] or macrocyclic[25,28] chelators. The $Mn^{2+}$ complexes are expected to be bishydrated, with all five ligand donor atoms lying in the equatorial plane and two water molecules occupying the axial positions of the pentagonal bipyramid (overall coordination number of seven). Such a coordination environment is commonly found in solid-state structures of the complexes with 15-membered macrocyclic ligands; however, in these cases, some of the apical positions are usually occupied by anion(s).[25,29] Nevertheless, bishydration was found in the solid state for the $Mn^{2+}$ complex of a *C*-substituted analogue of **L2**,[30] as well as for several complexes with related Schiff bases.[31] Recently, the bishydration was confirmed also in solution for $Mn^{2+}$ complexes of pentaaza macrocycles, including **L2**.[32] Importantly, since the two inner-sphere water molecules are situated in the axial positions on two opposite sides of the macrocycle plane, the formation of ternary complexes and, thus, the replacement of these waters by endogenous bidentate anions should not be important. Moreover, potentiometric data indicated reasonable stability for Mn**L2**.[25,32]

Here, we report several crystal structures of the free ligands and of Mn**L1** and Mn**L2** complexes. In solution, the ligand protonation constants and the thermodynamic stability constants of the complexes formed between **L1** or **L2** and various transition and alkaline earth metal ions were determined by pH-potentiometric titrations. In order to gain insight into the dissociation kinetics behavior of the Mn**L2** complex, we studied its transmetalation with $Zn^{2+}$. To the best of our knowledge, this is the first transmetalation study on a $Mn^{2+}$ complex. Finally, in order to assess the parameters governing proton relaxivity, variable-temperature $^{17}O$ NMR and $^{1}H$ NMRD measurements were performed on both $Mn^{2+}$ complexes. The formation of ternary complexes in the presence of some endogenous small anions was also investigated by relaxometric titrations.

In the following, the short formulas Mn**L1** or Mn**L2** will be used instead of the full formulas $[Mn(H_2O)_2(\mathbf{L1})]^{2+}$ or $[Mn(H_2O)_2(\mathbf{L2})]^{2+}$, respectively, for the complex cations, except the cases where the full formula is necessary.

## Experimental Section

**Synthesis. General.** Dry solvents were prepared by standard purification procedures,[33] distilled under argon, and stored over 4 Å molecular sieves in an argon atmosphere: THF (Penta, distilled from Na,K/benzophenone), $CHCl_3$ (Penta, distilled from $P_2O_5$), and MeOH (Penta, distilled from Na). The diethylester of pyridine-2,6-dicarboxylic acid,[34] 2,6-bis(hydroxymethyl)pyridine,[35] pyridine-2,6-dicarbaldehyde,[36] and the disodium salt of tetratosylated trien[37,38] and **L2**[39] were prepared according to the literature (or slightly modified, see the Supporting Information) procedures. Other solvents and chemicals were purchased from commercial sources and used as received.

(16) Koenig, S. H.; Baglin, C.; Brown, R. D., III; Brewer, C. F. *Magn. Reson. Med.* **1984**, *1*, 496–501.
(17) Troughton, J. S.; Greenfield, M. T.; Greenwood, J. M.; Dumas, S.; Wiethoff, A. J.; Wang, J.; Spiller, M.; McMurry, T. J.; Caravan, P. *Inorg. Chem.* **2004**, *43*, 6313–6323.
(18) Aime, S.; Anelli, P. L.; Botta, M.; Brocchetta, M.; Canton, S.; Fedeli, F.; Gianolio, E.; Terreno, E. *J. Biol. Inorg. Chem.* **2002**, *7*, 58–67.
(19) Maigut, J.; Meier, R.; Zahl, A.; van Eldik, R. *Inorg. Chem.* **2008**, *47*, 5702–5719.
(20) Bertin, A.; Steibel, J.; Michou-Gallani, A.-I.; Gallani, J.-L.; Felder-Flesch, D. *Bioconjugate Chem.* **2009**, *20*, 760–767.
(21) Geraldes, C. F. G. C.; Sherry, A. D.; Brown, R. D., III; Koenig, S. H. *Magn. Reson. Med.* **1986**, *3*, 242–250.
(22) Balogh, E.; He, Z.; Hsieh, W.; Liu, S.; Tóth, É. *Inorg. Chem.* **2007**, *46*, 238–250.
(23) Bianchi, A.; Calabi, L.; Giorgi, C.; Losi, P.; Mariani, P.; Palano, D.; Paoli, P.; Rossi, P.; Valtancoli, B. *J. Chem. Soc., Dalton Trans.* **2001**, 917–922.
(24) Wang, S.; Westmoreland, T. D. *Inorg. Chem.* **2009**, *48*, 719–728.
(25) Riley, D. P.; Henke, S. L.; Lennon, P. J.; Weiss, R. H.; Neumann, W. L.; Rivers, W. J., Jr.; Aston, K. W.; Sample, K. R.; Rahman, H.; Ling, C.-S.; Shieh, J.-J.; Busch, D. H.; Szulbinski, W. *Inorg. Chem.* **1996**, *35*, 5213–5231.
(26) Riley, D. P.; Schall, O. F. *Adv. Inorg. Chem.* **2006**, *59*, 233–263.
(27) Pellegatti, L.; Zhang, J.; Drahoš, B.; Villette, S.; Suzenet, F.; Guillaumet, G.; Petoud, S.; Tóth, É. *Chem. Commun.* **2008**, 6591–6593.
(28) (a) Tircsó, G.; Kovács, Z.; Sherry, A. D. *Inorg. Chem.* **2006**, *45*, 9269–9280. (b) Tircsó, G.; Tircsóné-Benyó, E.; Suh, E. H.; Jurek, P.; Kiefer, G. E.; Sherry, A. D.; Kovács, Z. *Bioconjugate Chem.* **2009**, *20*, 565–575.
(29) (a) Riley, D. P.; Weiss, R. H. *J. Am. Chem. Soc.* **1994**, *116*, 387–388. (b) Riley, D. P.; Lennon, P. J.; Neumann, W. L.; Weiss, R. H. *J. Am. Chem. Soc.* **1997**, *119*, 6522–6528. (c) Neumann, W. L.; Franklin, G. W.; Sample, K. R.; Aston, K. W.; Weiss, R. H.; Riley, D. P. *Tetrahedron Lett.* **1997**, *38*, 779–782.
(30) Liu, G.-F.; Filipović, M.; Heinemann, F. W.; Ivanović-Burmazović, I. *Inorg. Chem.* **2007**, *46*, 8825–8835.
(31) (a) Nishida, Y.; Tanaka, N.; Yamazaki, A.; Tokii, T.; Hashimoto, N.; Ide, K.; Iwasawa, K. *Inorg. Chem.* **1995**, *34*, 3616–3620. (b) Jimenez-Sandoval, O.; Ramirez-Rosales, D.; Rosales-Hoz, M. D. J.; Sosa-Torres, M. E.; Zamorano-Ulloa, R. *J. Chem. Soc., Dalton Trans.* **1998**, 1551–1556. (c) Marinescu, G.; Andruh, M.; Julve, M.; Lloret, F.; Llusar, R.; Uriel, S.; Vaissermann, J. *Cryst. Growth Des.* **2005**, *5*, 261–267. (d) Tu, H.-Y.; Liu, P.; Wang, C.-J.; Gao, M.-X.; Zhang, A.-D. *Mol. Cryst. Liq. Cryst.* **2007**, *469*, 79–87.
(32) Dees, A.; Zahl, A.; Puchta, R.; van Eikema Hommes, N. J. R.; Heinemann, F. W.; Ivanović-Burmazović, I. *Inorg. Chem.* **2007**, *46*, 2459–2470.
(33) *Purification of Laboratory Chemicals*; Perrin, D. D., Ed.; Pergamon Press: Oxford, U. K., 1988.
(34) Su, B.; Zhao, J. *Synth. Commun.* **2005**, *35*, 2317–2324.
(35) (a) Luning, U.; Baumstark, R.; Peters, K.; von Schenering, H. G. *Liebigs Ann. Chem.* **1990**, 129–143. (b) Ying, M.; Fubin, J.; Wei, H.; Xiangguang, M.; Xiaoqi, Y.; Xiancheng, Z. *J. Dispersion Sci. Technol.* **2006**, *27*, 15–21.
(36) (a) Papadopoulos, E. P.; Jarrar, A.; Issidorides, C. H. *J. Org. Chem.* **1966**, 615–616. (b) Hirano, M.; Yakabe, S.; Chikamori, H.; Clark, J. H.; Morimoto, T. *J. Chem. Res.* **1998**, 770–771.
(37) Meunier, I.; Mishra, A. K.; Hanquet, B.; Cocolios, P.; Guilard, R. *Can. J. Chem.* **1995**, *73*, 685–695.
(38) Bencini, A.; Fabbrizzi, L.; Poggi, A. *Inorg. Chem.* **1981**, *20*, 2544–2549.
(39) Stetter, H.; Frank, W.; Mertens, R. *Tetrahedron* **1981**, *37*, 767–772.

**Table 1.** Experimental Data of Reported Crystal Structures

| parameter | $(H_3\mathbf{L1})(ClO_4)_3$ | $(H_4\mathbf{L2})(ClO_4)_4\cdot H_2O$ | $[Mn(\mathbf{L1})(H_2O)Cl](ClO_4)$ | $[Mn(\mathbf{L1})(Cl)_2][Mn(\mathbf{L1})(H_2O)Cl]Cl\cdot 1.5H_2O$ | $[Mn(\mathbf{L2})(Cl)_2][Mn(\mathbf{L2})(H_2O)Cl]_2Cl_2\cdot 4H_2O$ |
|---|---|---|---|---|---|
| formula | $C_{13}H_{24}Cl_3N_3O_{14}$ | $C_{13}H_{29}Cl_4N_5O_{17}$ | $C_{13}H_{23}Cl_2MnN_3O_7$ | $C_{26}H_{47}Cl_4Mn_2N_6O_{6.50}$ | $C_{39}H_{81}Cl_6Mn_3N_{15}O_6$ |
| $M_r$ | 552.70 | 669.21 | 459.18 | 799.38 | 1233.71 |
| color and shape | colorless prism | colorless prism | light yellow rod | light yellow rod | light yellow prism |
| crystal system | triclinic | monoclinic | orthorhombic | orthorhombic | triclinic |
| space group | $P\bar{1}$ | $P2_1/c$ | $P2_12_12_1$ | $Pbca$ | $P\bar{1}$ |
| $a$/Å | 7.5939(9) | 16.8712(13) | 11.5773(2) | 23.9123(4) | 9.8317(10) |
| $b$/Å | 13.2091(9) | 16.5870(11) | 12.0710(3) | 10.13720(10) | 16.3981(19) |
| $c$/Å | 32.582(3) | 24.3079(12) | 13.5727(3) | 28.3187(4) | 18.5489(14) |
| $\alpha$/deg | 89.331(8) | 90 | 90 | 90 | 103.283(8) |
| $\beta$/deg | 83.689(10) | 132.670(7) | 90 | 90 | 100.198(8) |
| $\gamma$/deg | 78.320(8) | 90 | 90 | 90 | 95.355(8) |
| $U$/Å$^3$ | 3181.0(5) | 5001.6(6) | 1896.78(7) | 6864.56(16) | 2836.3(5) |
| $Z$ | 6 | 8 | 4 | 8 | 2 |
| $D_c$/g cm$^{-3}$ | 1.731 | 1.777 | 1.608 | 1.547 | 1.445 |
| $\mu$/mm$^{-1}$ | 0.512 | 0.565 | 1.018 | 1.097 | 0.995 |
| $R_1$ [$I \geq 2\sigma(I)$]; $R_2$ (all data)[a] | 0.1762; 0.1904 | 0.0489; 0.1028 | 0.0301; 0.0674 | 0.0339; 0.0732 | 0.1477; 0.3517 |
| $wR_1$ [$I \geq 2\sigma Z(I)$]; w$R_2$ (all data)[a] | 0.3809; 0.3880 | 0.0823; 0.1240 | 0.0359; 0.0708 | 0.0482; 0.0802 | 0.1752; 0.3654 |

[a] $R_1$, $R_2 = \sum|F_o - F_c|/\sum|F_c|$; $wR_1$, $wR_2 = [\sum w(F_o^2 - F_c^2)^2/\sum w(F_o^2)^2]^{1/2}$ (ref 44).

NMR spectra were recorded on a Varian VNMRS300 spectrometer at 25 °C: $^1$H 299.9 MHz, TMS (internal) $\delta = 0.00$ ppm; $^{13}$C 75.4 MHz, TMS (internal) $\delta = 0.00$ ppm; $CHCl_3$ (internal) $\delta = 77.00$ ppm. Multiplicity of the signals is indicated as follows: s, singlet; d, doublet; t, triplet; q, quartet; m, multiplet; br, broad. Deuterated solvent $CDCl_3$ (99.8% D) from Chemtrade was used as received. Mass spectra were measured on a Bruker spectrometer ESQUIRE 3000 equipped with an electro-spray ion source and ion-trap detector in positive/negative mode and on an Autoflex instrument (Bruker Daltonics, Bremen, Germany) using the MALDI-TOF ionization/detection technique. For thin layer chromatography, Merck aluminum foils with silica gel 60 F254 impregnated with a fluorescent dye were used. Elemental analyses were done at the Institute of Macromolecular Chemistry (Academy of Science of the Czech Republic, Prague).

**3,12,18-Triaaza-6,9-dioxabicyclo[12.3.1]octadeca-1(18),14,16-triene (L1, 15-py$N_3O_2$).**[40,41] Pyridine-2,6-dicarbaldehyde (1.50 g, 11.1 mmol) and $MnCl_2\cdot 4H_2O$ (2.18 g, 11.0 mmol) were dissolved in dry MeOH (150 mL). The solution of 1,8-diamino-3,6-dioxaoctane (1.66 g, 11.2 mmol) in dry MeOH (25 mL) was added dropwise over 15 min. The yellow reaction mixture was heated for 2 h at 60 °C and became light brown. After cooling to 0 °C, $NaBH_4$ (5.61 g, 148.3 mmol) was added portionwise. The solution was left stirring overnight at RT. Water (50 mL) was slowly added, inducing precipitation of $Mn(OH)_2$ (which started to oxidize), and this suspension was stirred at RT for 1 h. MeOH was removed *in vacuo*, and the remaining aqueous phase was extracted with $CH_2Cl_2$ (3 × 50 mL). The organic layer was dried with anhydrous sodium sulfate, and the solvent was evaporated under reduced pressure. The crude product was purified by column chromatography ($SiO_2$, EtOH/$NH_3$(aq.) 20:1, $R_f = 0.3$) and dried *in vacuo* at 50 °C to obtain a yellowish oil (2.06 g, 74% based on pyridine-2,6-dicarbaldehyde).

$^1$H NMR ($CDCl_3$): $\delta$ 2.65 (N**H**, 2H, br s); 2.75 (OC$\mathbf{H}_2$C$\mathbf{H}_2$N, 4H, m); 3.51 (OC$\mathbf{H}_2$C$\mathbf{H}_2$O, 4H, s); 3.58 (OC$\mathbf{H}_2$C$\mathbf{H}_2$N, 4H, m); 3.81 (NC$\mathbf{H}_2$py, 4H, s); 6.90 (C**H** arom., 2H, d, $^3J_{HH} = 7.8$ Hz); 7.42, (C**H** arom., 1H, t, $^3J_{HH} = 7.8$ Hz). $^{13}$C{$^1$H} NMR: $\delta$ 49.0 (C$\mathbf{H}_2$−N, 2C); 53.2 (C$\mathbf{H}_2$−N, 2C); 69.5 (C$\mathbf{H}_2$−O, 2C), 70.1 (C$\mathbf{H}_2$−O, 2C); 120.4 (C**H** arom., 2C); 136.9 (C**H** arom., 1C); 156.9 (**C**-$CH_2$, 2C). MS, $m/z$ (+): 252.0 $(L+H)^+$; 274.0 $(L+Na)^+$. Elemental analysis for $C_{13}H_{21}N_3O_2\cdot C_2H_5OH\cdot 3H_2O$ found (calculated): C, 50.86 (51.26); H, 8.11 (9.46); N, 11.68 (11.96).

**Crystal Structure Determination.** Single crystals of the perchlorate salts of the free ligands were obtained by slow cooling of a saturated aqueous ligand solution, acidified by several drops of perchloric acid (conc. 65%). The solutions of the complexes were prepared by mixing an aqueous ligand solution ($c_L = 17$ mM) and manganese(II) chloride or manganese(II) perchlorate ($c_{Mn} = 99$ or 157 mM) in a Mn/L molar ratio of 1:1.05. The solutions were evaporated to dryness under reduced pressure, and the residue was dissolved in EtOH. The single crystals for the X-ray analysis were prepared by a slow vapor diffusion of $Et_2O$ into the ethanol solution of the Mn(II) complexes at 5 °C.

Selected crystals were mounted on a glass fiber in random orientation and cooled to 150(1) K. The diffraction data were collected on a Nonius Kappa CCD diffractometer (Enraf-Nonius) using Mo $K_\alpha$ ($\lambda = 0.71073$ Å) at 150(1) K (Cryostream Cooler Oxford Cryosystem) and analyzed with the HKL DENZO program package.[42] The structures were solved by direct methods and refined by full-matrix least-squares techniques [SIR92 (ref 43) and SHELXL97 (ref 44)]. The scattering factors used for neutral atoms were included in the SHELXL97 program. Selected experimental data are listed in Table 1.

In the structure of $(H_3\mathbf{L1})(ClO_4)_3$, three protonated ligand molecules and nine perchlorate anions form the independent unit. The hydrogen atoms were located in the electron density difference map; however, they were fixed in theoretical positions using $U_{eq}(H) = 1.2U_{eq}(X)$. The residual maxima of electronic density lay very close to chlorine/oxygen atoms, pointing to a disorder of the corresponding perchlorate anions. These disorders could be reliably modeled only in the case of three anions. All non-hydrogen atoms were refined anisotropically, except for several atoms of one macrocycle unit which became nonpositive-definite, and except for disordered (not fully occupied) perchlorate oxygen atoms; these atoms were treated isotropically. In the crystal structure, there is still a number of residual density peaks (1−2 e A$^{-3}$, the largest ones are nonreliable close

(40) Storm, O.; Lüning, U. *Chem.—Eur. J.* **2002**, *8*, 793–798.
(41) Bonadio, F.; Senna, M.-C.; Ensling, J.; Sieber, A.; Neels, A.; Stoeckli-Evans, H.; Decurtins, S. *Inorg. Chem.* **2005**, *44*, 969–978.
(42) (a) Otwinovski, Z; Minor, W. *HKL Denzo and Scalepack Program Package*; Nonius BV: Delft, The Netherlands, 1997. (b) Otwinovski, Z.; Minor, W. *Methods Enzymol.* **1997**, *276*, 307–326.
(43) Altomare, A.; Burla, M. C.; Camalli, M.; Cascarano, G.; Giacovazzo, C.; Guagliardi, A.; Polidori, G. *J. Appl. Crystallogr.* **1994**, *27*, 435–435.
(44) Sheldrick, G. M. *SHELXL97*; University of Göttingen: Göttingen, Germany, 1997.

to the chlorine/oxygen atoms, pointing to a disorder in the perchlorate fragments), which decrease the quality of the statistical parameters of the refinement. Those maxima are probably artifacts of a low crystal quality. However, the structure of the ligand molecules could be determined unambiguously as evidenced by the reasonable values of the bonding parameters.

In the structure of $(H_4\mathbf{L2})(ClO_4)_4 \cdot H_2O$, two independent ligand molecules were found. All non-hydrogen atoms were refined anisotropically. The hydrogen atoms, including those attached to water oxygen atoms, were located in the electron density difference map; however, they were fixed in theoretical (C−H, N−H) or original (O−H) positions using $U_{eq}(H) = 1.2U_{eq}(X)$. In the structure, there are eight independent perchlorate anions. The highest maximum of residual electronic density lays very close to one of the chlorine atoms, pointing to a slight disorder of the corresponding perchlorate anion. This disorder cannot be appropriately modeled.

In the crystal structure of $[Mn(\mathbf{L1})(H_2O)Cl](ClO_4)$, all non-hydrogen atoms were refined anisotropically. The hydrogen atoms, including those attached to water oxygen atoms, were located using the electron density difference map; however, they were fixed in theoretical (C−H, N−H) or original (O−H) positions using $U_{eq}(H) = 1.2U_{eq}(X)$. As this compound crystallized in a noncentrosymmetric space group $P2_12_12_1$, only one enantiomer was present in the crystal structure (the chirality of the molecule is brought by the torsion of the five-membered chelate rings, which is, going from the pyridine nitrogen atom, $\delta\lambda\delta\lambda\delta$). Chirality was assigned using a possibility with Flack's parameter equal to zero. However, principally, both enantiomers must be formed during the complexation reaction, as there was no source of chirality in the reaction mixture.

In the crystal structure of $[Mn(\mathbf{L1})(Cl)_2][Mn(\mathbf{L1})(H_2O)Cl]Cl \cdot 1.5H_2O$, all non-hydrogen atoms were refined anisotropically. The largest maximum in the electronic difference map was assigned to the chloride anion, and the four remaining high difference electronic maxima isolated were best refined as disordered solvate water molecules. Two larger (very close) maxima were interpreted as one molecule with full occupancy, and two neighboring, less intense maxima were attributed to half-occupied water molecules. Hydrogen atoms were located using the electron density difference map; however, they were fixed in theoretical (C−H, N−H) or original (O−H) positions using $U_{eq}(H) = 1.2U_{eq}(X)$.

In the structure of $[Mn(\mathbf{L2})(Cl)_2][Mn(\mathbf{L2})(H_2O)Cl]_2Cl_2 \cdot 4H_2O$, three independent complex units were found, two monoaqua-monochlorido and one dichlorido species, together with two chloride anions. Several remaining electronic density maxima were attributed to solvate water molecules, one of them disordered in two positions. All non-hydrogen atoms (except of disordered water solvate) were refined anisotropically. Despite the low quality of the crystal data, most of the hydrogen atoms could be located in the electronic density map; however, they were fixed in theoretical (C−H, N−H) or original (O−H) positions using $U_{eq}(H) = 1.2U_{eq}(X)$. In the crystal structure, there is still a number of residual density peaks (1−2 e $A^{-3}$, the largest ones are nonreliable, close to the manganese(II) ions), which decrease the quality of the statistical parameters of the refinement, but they are probably artifacts of a low crystal quality and cannot be reasonably interpreted. Nevertheless, the structure of the complexes could be determined unambiguously, even with reasonable esd's of the bond parameters.

**Potentiometric Measurements.** To determine the protonation constants of the ligands and the stability constants of their complexes formed with different metal ions, potentiometric titrations were carried out at a 1:1 metal-to-ligand molar ratio. Titrations were performed at 25.0 ± 0.1 °C and at an ionic strength of $I = 0.1$ M ($NMe_4Cl$) using deionized water. An inert atmosphere was provided by a constant passage of argon saturated with the solvent vapor. The titrations were run in the $-\log[H^+]$ range from 1.8 (**L1**) or 2.5 (**L2**; except $Cu^{2+}$ starting at $-\log[H^+]$ 1.6) to 11.8 (or until precipitation of the metal hydroxide) with an extra HCl added to the starting solution. A PHM 240 pH-meter, a 2-mL ABU 901 automatic piston buret, and a GK 2401B combined electrode (all Radiometer, Denmark) were used. The initial volume in the titration cell was 5 mL. Titrations were performed with a $NMe_4OH$ solution (~0.2 M), and the concentration of the ligand in the titrated solutions was ~0.004 M. For each system, four parallel titrations were carried out, one titration consisting of about 50 points. All equilibria were established quickly. For calculations, the OPIUM software package was used.[45] The value of $pK_w$ was 13.81. The stability constants of the $M^{2+}-OH^-$ systems were taken from the literature.[46] For more details about potentiometric titrations, see previous papers.[47] In the followings, pH will mean $-\log[H^+]$ and all the equilibrium constants are concentration constants.

**Sample Preparation for NMR Measurements.** The $Mn^{2+}$ complexes have been prepared by mixing solutions of $MnCl_2$ or $Mn(ClO_4)_2$ and the ligand (in 10% molar excess) and adjusting the pH to 8.0. Mn**L1**, MS $m/z$ (+): 341.1 (Mn**L1**Cl)$^+$; 494.0 (Mn**L1**(CCA))$^+$. Mn**L2**, MS $m/z$ (+): 339.1 (Mn**L2**Cl)$^+$; 492.1 (Mn**L2**(CCA))$^+$ (HCCA = α-cyano-4-hydroxycinnamic acid). ***Caution!*** *Dry powder perchlorate samples, especially in larger quantities, should be handled with great care.*

**$^{17}$O NMR Measurements.** Variable-temperature $^{17}$O NMR measurements of aqueous solutions of Mn**L1** or Mn**L2** ($c_{MnL}$ = 5 mmol/kg, pH 8.0, in 0.1M TRIS buffer; TRIS = tris-(hydroxomethyl)aminomethane) were performed on a Bruker Avance 500 MHz spectrometer (11.7 T, 67.8 MHz) in the temperature range 0−85 °C. The temperature was calculated according to previous calibration with ethylene glycol and MeOH.[48] Acidified water ($HClO_4$, pH = 3.3) or the corresponding $Zn^{2+}$ complex at identical concentration and pH as the paramagnetic $Mn^{2+}$ sample were used as standard diamagnetic references, and they gave identical results, as in previous studies. The $^{17}$O longitudinal ($T_1$) and transverse ($T_2$) relaxation times were obtained by the inversion−recovery pulse sequence[49] and Carl−Purcell−Meiboom−Gill spin−echo technique, respectively.[50] To eliminate the susceptibility corrections to the chemical shift[51] the sample was placed in a glass sphere fixed in a 10 mm NMR tube. To improve sensitivity, the amount of $^{17}$O was enriched by adding $H_2{}^{17}O$ (10% $H_2{}^{17}O$, CortecNet) to achieve approximately 1% $^{17}$O content in the sample.

**NMRD Measurements.** The $^1$H NMRD profiles of aqueous $Mn^{2+}$ complex solutions ($c_{Mn2+}$ = 5 mM, pH 8.0, 0.1 M TRIS buffer) were measured at 25, 37, 50, and 65 °C on a Stelar SMARTracer Fast Field Cycling NMR relaxometer (0.00024−0.24 T, 0.01−10 MHz $^1$H Larmor frequency) and a Bruker

(45) (a) Kývala, M.; Lukeš, I. International Conference Chemometrics '95, Pardubice, Czech Republic, **1995**, p 63. (b) Kývala, M.; Lubal, P.; Lukeš, I. IX. Spanish−Italian and Mediterranean Congress on Thermodynamics of Metal Complexes (SIMEC 98), Girona, Spain, **1998**. The full version of the OPIUM program is available (free of charge) on http://www.natur.cuni.cz/_kyvala/opium.html.

(46) (a) Martell, A. E.; Smith, R. M. *Critical Stability Constants*; Plenum Press: New York, 1974−1989; Vols. *1*−*6*. (b) *NIST Standard Reference Database 46* (*Critically Selected Stability Constants of Metal Complexes*), Version 7.0; NIST: Gaithersburg, MD, **2003**. (c) Baes, C. F., Jr.; Mesmer, R. E. *The Hydrolysis of Cations*; Wiley: New York, 1976.

(47) (a) Táborský, P.; Lubal, P.; Havel, J.; Kotek, J.; Rudovský, J.; Hermann, P.; Lukeš, I. *Collect. Czech. Chem. Commun.* **2005**, *70*, 1909–1942. (b) Försterová, M.; Svobodová, I.; Lubal, P.; Táborský, P.; Kotek, J.; Hermann, P.; Lukeš, I. *Dalton Trans.* **2007**, 535–549.

(48) Raiford, D. S.; Fisk, C. L.; Becker, E. D. *Anal. Chem.* **1979**, *51*, 2050–2051.

(49) Vold, R. L.; Waugh, J. S.; Klein, M. P.; Phelps, D. E. *J. Chem. Phys.* **1968**, *48*, 3831–3832.

(50) Meiboom, S.; Gill, D. *Rev. Sci. Instrum.* **1958**, *29*, 688–691.

(51) Hugi, A. D.; Helm, L.; Merbach, A. E. *Helv. Chim. Acta* **1985**, *68*, 508–521.

**Scheme 1.** Synthesis of Ligand **L1**: (i) $MnCl_2$, MeOH, 60 °C, 2 h; (ii) 1. $NaBH_4$; 2. $H_2O$ on air

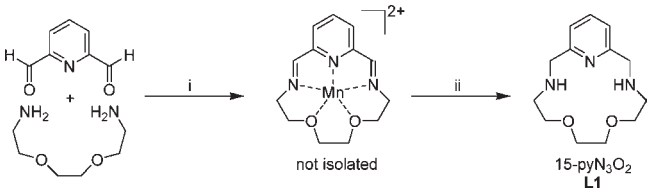


WP80 NMR electromagnet adapted to variable-field measurements (0.47−1.88 T, 20−80 MHz $^1$H Larmor frequency) and controlled by the SMARTracer PC-NMR console. The temperature was controlled by a VTC91 temperature control unit and maintained by a gas flow. It was determined according to previous calibration with a Pt resistance temperature probe. The relaxivity at 500 MHz was measured on a Bruker Avance 500 (11.75 T) spectrometer. The temperature was calculated according to the previous calibration with ethylene glycol and MeOH.[48]

**Anion Binding Study.** To assess ternary complex formation with small endogenous anions, relaxometric titrations were carried out on a Stelar SMARTracer Fast Field Cycling NMR relaxometer at 0.5 MHz and 25 °C. A solution of the anion ($c_{(phosphate)} = c_{(carbonate)} = c_{(citrate)} = 100$ mM) was added stepwise to 1 mL of the $Mn^{2+}$ complex solution ($c_{Mn2+} = 1$ mM, 0.1 M TRIS buffer, pH 8.0) up to 100 equivalents of the anion.

**Dissociation Kinetics.** The transmetalation of Mn**L2** with $Zn^{2+}$ was followed by monitoring the relaxivity at 0.5 MHz on a Stelar SMARTracer Fast Field Cycling relaxometer ($c_{Mn2+} =$ 1 mM, 0.02 M MES buffer; MES = 2-(4-morpholino)ethanesulfonic acid) in the pH range 4.7−6.0 and in the presence of 5-, 10-, 20-, 30-, and 50-fold excesses of the exchanging $Zn^{2+}$ at 25 °C and 0.1 M KCl.

**Data Evaluation.** The analysis of the experimental $^{17}$O NMR, $^1$H NMRD, and kinetic data was performed with the Micromath Scientist program (version 2.0, Salt Lake City, UT) using a least-squares fitting procedure.[52]

## Results and Discussion

**Syntheses.** The crucial precursor for the synthesis of **L1**, pyridine-2,6-dicarbaldehyde, was prepared from the commercially available pyridine-2,6-dicarboxylic acid by its esterification to diethyl ester,[34] subsequent reduction by $NaBH_4$ to 2,6-bis(hydroxymethyl)pyridine,[35] and gentle selective oxidation employing $MnO_2$.[36] The last two reaction steps were slightly modified with respect to literature procedures (see the Supporting Information) where, in particular, the purification procedures were improved.

Ligand **L1** was previously prepared by the template reaction on $Mg^{2+}$.[40] To facilitate the procedure and, mainly, to avoid the high-dilution technique, the template reaction on $Mn^{2+}$ was employed (Scheme 1). The reaction conditions were similar to those previously described for the preparation of $Mn^{2+}$ complexes with a Schiff-base derived from 2,6-diacetylpyridine and different amines or aminoethers.[41] After reduction of the $Mn^{2+}$ Schiff base complex (not isolated) with $NaBH_4$ and hydrolysis of the hydride excess, the manganese precipitated in the form of $Mn(OH)_2$ and was further oxidized in the air allowing a simple demetalation to obtain the free ligand which was purified by column chromatography. The additional purification could be done by a high-vacuum distillation ($< 10^{-2}$ mbar). The overall yield was 74%.

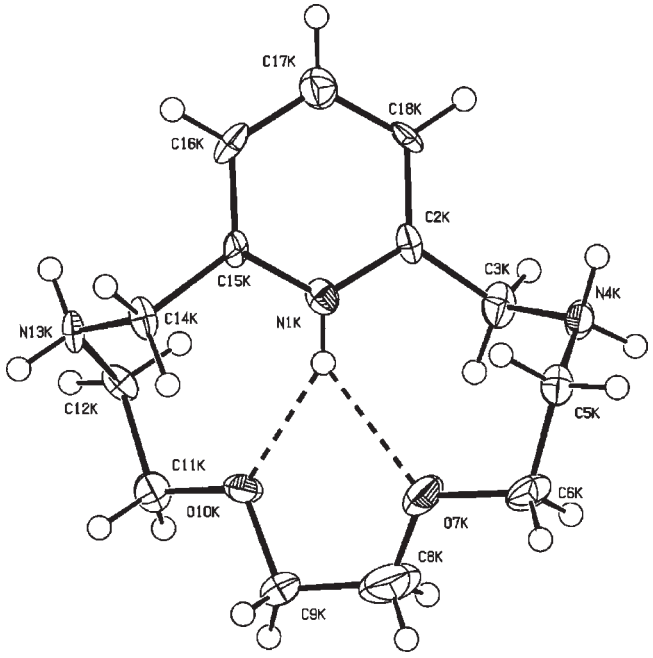


**Figure 1.** Molecular structure of one of the $(H_3\mathbf{L1})^{3+}$ cations found in the structure of $H_3\mathbf{L1}(ClO_4)_3$ showing intramolecular hydrogen bonds. The thermal ellipsoids are drawn with 50% probability.

The manganese(II) complex of **L2** (which could be demetalated as above) has also been prepared directly by the analogous template synthesis but in a rather low yield.[32] In our hands, any attempts to reproduce the synthesis failed, giving only nonpurifiable reaction mixtures. Therefore, the general Atkins-Richman procedure was used for the synthesis of the macrocycle.[39] The procedure was slightly modified (Supporting Information). The MS spectrum after the deprotection showed only the molecular ion of the pure product, but there were two spots on TLC. To ensure the purity of **L2**, column chromatography was performed, and the final product was obtained in a 42% overall yield as a light-yellow solid (Supporting Information).

**Crystal Structures. Crystal Structures of the Free Ligands.** In the structure of $H_3\mathbf{L1}(ClO_4)_3$, three independent ligand molecules were found, adopting very close geometries. Therefore, only one of them is shown in Figure 1. The molecules have a propeller-like shape, with a pseudo-$C_2$ symmetry axis passing through carbon C17, nitrogen N1, and the center of the C8−C9 bond. All amino groups (secondary amines and the pyridine nitrogen) were found to be protonated. The protonation of the pyridine nitrogen atom N1 is stabilized by two medium-strong hydrogen bonds involving the macrocycle oxygen atoms O7 and O10, with $d_{N\cdots O} \sim 2.8-3.0$ Å. Such a hydrogen bond system results in a twisting of the macrocycle cavity. The protonated secondary amino groups contribute to an extended hydrogen bond system involving oxygen atoms of the perchlorate counterions. However, several perchlorates have no hydrogen-bond contacts, resulting in a disorder of some of these anions.

In the crystal structure of $H_4\mathbf{L2}(ClO_4)_4 \cdot H_2O$, two independent ligand molecules were found, adopting very similar conformations; therefore, only one of them is

(52) *Scientist for Windows*, version 2.0; Micromath Inc.: Salt Like City, UT, 1995.

shown in Figure 2. The molecules have rectangular geometry, with corners in the atoms C3, N7, N10, and C14. All secondary amino groups are protonated, but not the pyridine unit. In the independent unit, there are eight perchlorate anions, which form an extended medium-strong hydrogen bond network with protonated amino groups and solvate water molecules.

**Crystal Structures of the MnL1 Complexes.** In the structure of $[Mn(\mathbf{L1})(Cl)_2][Mn(\mathbf{L1})(H_2O)Cl]Cl\cdot 1.5H_2O$, two independent complex units were found, having the central $Mn^{2+}$ ion coordinated in the center of the planar macrocyclic cavity, with two other donor atoms in apical positions forming the pentagonal-bipyramidal coordination spheres. The two units differ in apically coordinating groups: in the first unit, the $Mn^{2+}$ is coordinated by two chloride anions, while in the second unit, one apical site is occupied by a chloride and the coordination sphere is completed by a water molecule (Figure 3).

In an attempt to characterize the bishydrated complex, we also used perchlorate as a counteranion with low coordination ability (i.e., $Mn(ClO_4)_2$ as the starting salt, mixed with anion-free ligand). Only very few crystals suitable for the X-ray diffraction were isolated from this mixture. To our surprise, the X-ray analysis revealed that the crystal contains chloride and has a composition of $[Mn(\mathbf{L1})(H_2O)Cl](ClO_4)$, with almost identical geometric parameters as the $[Mn(\mathbf{L1})(H_2O)Cl]^+$ unit found in the previous structure. It evidences that the presence of chloride is essential for a successful crystallization.

All three Mn**L1** complex units have very similar pseudo-$C_2$ geometry of the macrocyclic part, with virtual 2-fold axes laying on the Mn−N(pyridine) coordination bond. The 5-fold chelate rings adopt alternate $\delta/\lambda$ conformations; in the case of the chiral $[Mn(\mathbf{L1})(H_2O)Cl](ClO_4)$ complex, the chirality of the chelate rings (starting from the pyridine nitrogen atom) was $\delta\lambda\delta\lambda\delta$; therefore, independent molecules with the same chirality were chosen also in the centrosymmetric structure of $[Mn(\mathbf{L1})(Cl)_2][Mn(\mathbf{L1})(H_2O)Cl]Cl\cdot 1.5H_2O$ to have analogous signs of the torsion angles.

The molecular structure of the $[Mn(\mathbf{L1})(H_2O)Cl]^+$ cation found in the structure of $[Mn(\mathbf{L1})(H_2O)Cl](ClO_4)$ is shown in Figure S1 (Supporting Information), and selected geometric parameters are listed in Table 2 and Tables S1 and S2 (Supporting Information).

**Crystal Structure of MnL2.** In the structure of the Mn**L2** complex, three independent complex units were found, one dichlorido and two monoaqua-monochlorido units, giving the formula $[Mn(\mathbf{L2})(Cl)_2][Mn(\mathbf{L2})(H_2O)Cl]_2Cl_2\cdot 4H_2O$. All molecules have a pentagonal-bipyramidal shape, with five macrocycle nitrogen atoms in the equatorial and two other donors (chloride and water molecule) in the apical positions, similarly to the previous structures of Mn**L1** complexes. Figure 4 shows the drawing of $[Mn(\mathbf{L2})(Cl)_2]$ and one of the $[Mn(\mathbf{L2})(H_2O)Cl]^+$ cations found in this crystal structure. As the compound crystallized in the centrosymmetric unit, the independent part was chosen in accordance with the previous cases of Mn**L1** (see above) to have $\delta\lambda\delta\lambda\delta$ conformation of the chelate rings, in order to obtain directly comparable values for the macrocycle torsion angles (Table S2, Supporting Information). All independent macrocyclic fragments have a virtual 2-fold symmetry, similarly to the previous case. Other structural features are also very similar (Table 2 and Tables S1 and S2, Supporting Information).

**Structural Features of the $Mn^{2+}$ Complexes.** All coordination bonds (Table 2) lay in the expected range, similarly to those found in related structures.[29,30] The

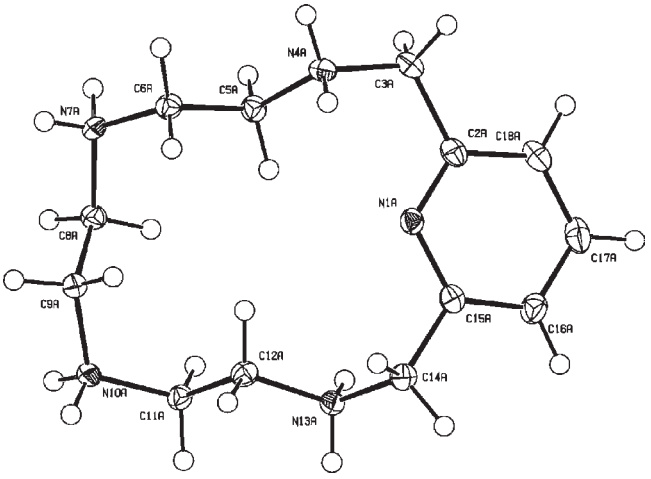


**Figure 2.** Molecular structure of one of the $(H_4\mathbf{L2})^{4+}$ cations found in the structure of $H_4\mathbf{L2}(ClO_4)_4\cdot H_2O$. The thermal ellipsoids are drawn with 50% probability.

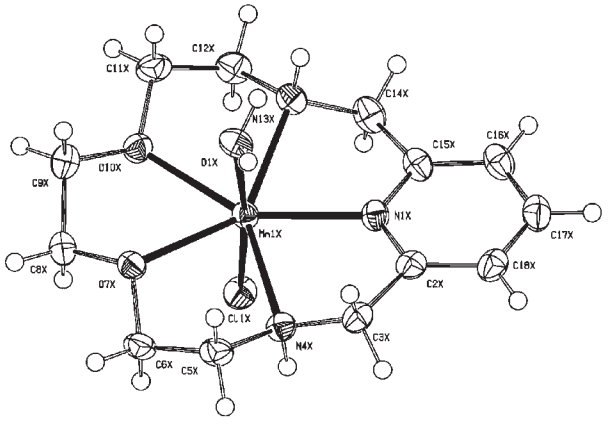


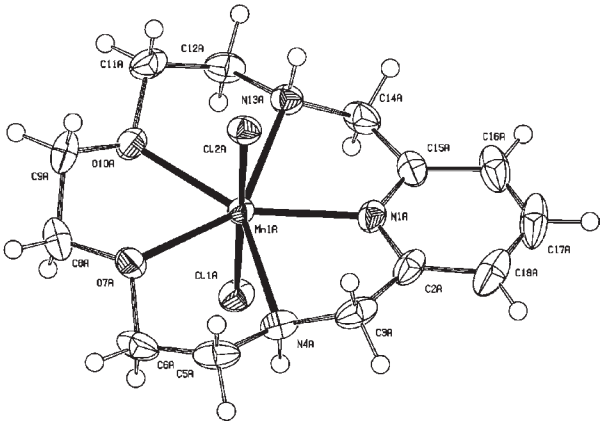


**Figure 3.** Molecular structures of the $[Mn(\mathbf{L1})(Cl)_2]$ and $[Mn(\mathbf{L1})(H_2O)Cl]^+$ complex units found in the structure of $[Mn(\mathbf{L1})(Cl)_2][Mn(\mathbf{L1})(H_2O)Cl]Cl\cdot 1.5H_2O$. The thermal ellipsoids are drawn with 50% probability.

**Table 2.** Selected Interatomic Distances (Å) and Bond Angles (deg) Found in the Crystal Structures of [Mn(**L1**)($H_2O$)Cl]($ClO_4$), [Mn(**L1**)$(Cl)_2$][Mn(**L1**)($H_2O$)Cl]Cl·1.5$H_2O$, and [Mn(**L2**)$(Cl)_2$]-[Mn(**L2**)($H_2O$)Cl]$_2Cl_2$·4$H_2O$

| compound | [Mn(**L1**)($H_2O$)Cl]-($ClO_4$) | [Mn(**L1**)$(Cl)_2$][Mn(**L1**)-($H_2O$)Cl]Cl·1.5$H_2O$ | | [Mn(**L2**)$(Cl)_2$][Mn(**L2**)-($H_2O$)Cl]$_2Cl_2$·4$H_2O$ | | |
|---|---|---|---|---|---|---|
| unit | [Mn(**L1**)($H_2O$)Cl]$^+$ | [Mn(**L1**)$(Cl)_2$] | [Mn(**L1**)($H_2O$)Cl]$^+$ | [Mn(**L2**)$(Cl)_2$] | [Mn(**L2**)($H_2O$)Cl]$^+$ | [Mn(**L2**)($H_2O$)Cl]$^+$ |
| | | | Distances (Å) | | | |
| Mn−N1 | 2.229(2) | 2.218(2) | 2.219(2) | 2.268(10) | 2.267(10) | 2.267(10) |
| Mn−N4 | 2.334(2) | 2.319(2) | 2.316(2) | 2.342(10) | 2.345(9) | 2.328(10) |
| Mn−(O7,N7)[a] | 2.250(2) | 2.290(2) | 2.299(2) | 2.307(10) | 2.319(10) | 2.334(10) |
| Mn−(O10,N10)[a] | 2.305(2) | 2.295(2) | 2.315(2) | 2.323(10) | 2.332(10) | 2.368(11) |
| Mn−N13 | 2.300(2) | 2.284(2) | 2.313(2) | 2.340(10) | 2.346(10) | 2.364(10) |
| Mn−Cl1 | 2.5073(6) | 2.4997(7) | 2.5026(7) | 2.586(3) | 2.588(3) | 2.547(3) |
| Mn−Cl2 | | 2.6325(7) | | 2.623(4) | | |
| Mn−Ow[b] | 2.230(2) | | 2.287(2) | | 2.295(10) | 2.267(9) |
| Mn−H1w | 2.758 | | 2.786 | | 2.758 | 2.742 |
| Mn−H2w | 2.775 | | 2.796 | | 2.862 | 2.977 |
| $d(N_3O_2/N_5)$−Mn[c] | −0.1325(9) | −0.0715(9) | −0.1218(9) | −0.022(5) | −0.038(5) | −0.065(5) |
| $d(N_3O_2/N_5)$−Cl1[c] | −2.6398(10) | −2.5688(10) | −2.6215(10) | 2.595(6) | −2.623(6) | −2.612(5) |
| $d(N_3O_2/N_5)$−Cl2[c] | | 2.5585(10) | | −2.606(5) | | |
| $d(N_3O_2/N_5)$−Ow[b,c] | 2.090(2) | | 2.161(2) | | 2.253(10) | 2.201(10) |
| | | | Angles (deg) | | | |
| Cl1−Mn1−Cl2(Ow)[d] | 175.12(5) | 176.32(2) | 173.99(4) | 178.2(1) | 176.6(3) | 178.3(3) |

[a] (O7,N7) and (O10,N10) give alternative atoms in ligands **L1** and **L2**, respectively. [b] Ow stays for coordinated water oxygen atom. [c] $d(N_3O_2/N_5)$−X is the distance of the atom X from the macrocyclic plane, defined by coordinating atoms. [d] Cl1−Mn1−Cl2 in the bis(chlorido) and Cl1−Mn1−Ow in aqua-chlorido complex species, respectively.

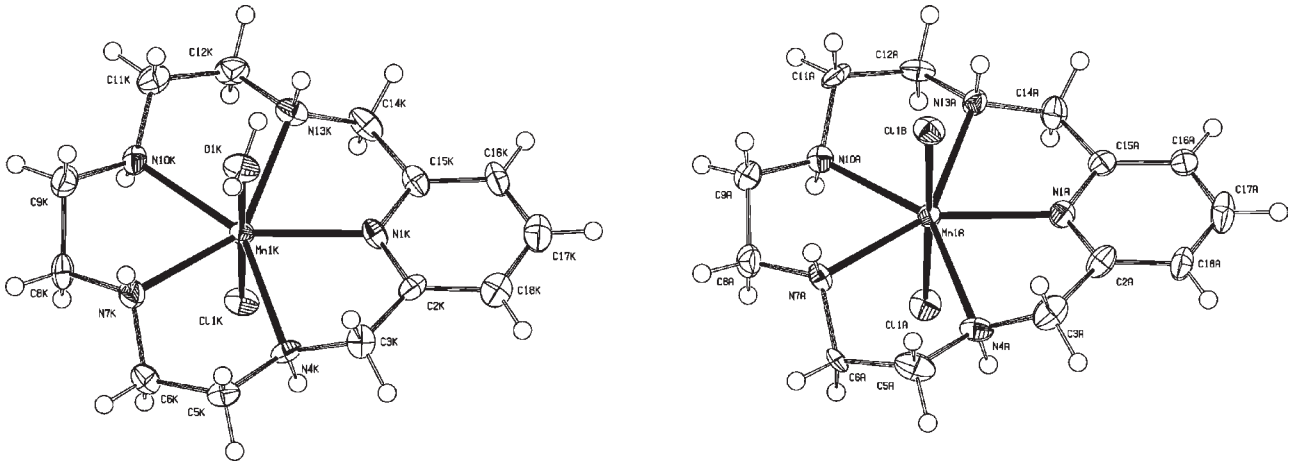


**Figure 4.** Molecular structures of the [Mn(**L2**)$(Cl)_2$] complex unit and of one of the [Mn(**L2**)($H_2O$)Cl]$^+$ cations found in the structure of [Mn(**L2**)$(Cl)_2$][Mn(**L2**)($H_2O$)Cl]$_2Cl_2$·4$H_2O$. The thermal ellipsoids are drawn with 50% probability.

distances N(pyridine)−Mn (~2.22−2.27 Å) are slightly shorter as compared to other N−Mn bonds (2.28−2.37 Å). The coordination bonds between the macrocycle oxygen atom and the central ion are 2.25−2.32 Å, on average only slightly longer than coordination bonds between the coordinated water molecule and the $Mn^{2+}$ (2.23−2.29 Å). The distances between the hydrogen atoms of the coordinated water and the $Mn^{2+}$ are in the range of 2.74−2.98 Å. The Cl−Mn coordination bonds are 2.50−2.63 Å long. The macrocyclic ligand forms a slightly distorted pentagonal plane, with a deviation of the donor atoms from the mean plane in the range of 0.0−0.3 Å. In the mixed aqua-chlorido species, the central $Mn^{2+}$ lays slightly above this plane toward the chloride anions. In the bis(chlorido) species, the central ion lays more regularly within the macrocyclic plane. The bond angles between two neighboring donor atoms in the equatorial plane and the central $Mn^{2+}$ ion are in the range of 69.6−76.1° (Table S1, Supporting Information), consistent with the theoretical value of 72.0° for a regular pentagon. Both ligands adopt almost the same conformation in the equatorial plane (Table S2, Supporting Information). The bond angle between apical donor atoms is 174.0−178.3°, which corresponds well to a regular *trans*-apical coordination.

**Thermodynamic Study.** Stepwise protonation constants of **L1** and **L2** as well as stability constants of their complexes with various transition and alkaline earth metal ions were determined by standard potentiometric titrations (Tables 3 and 4). The Mn**L2** complex has been previously investigated.[25,32] In the case of the $Co^{2+}$−**L2** system, metal ion oxidation prevented the titration. A full set of the experimental values (with standard deviations) is given in the Supporting Information (Table S3).

As expected, two protonation constants were found for **L1**, corresponding to the secondary amine nitrogen

atoms. The third protonation constant, probably related to the pyridine nitrogen, is too low to be detected under our experimental conditions. For **L2**, the three protonation constants observed are in good agreement with previously measured data.[25,32] They correspond to the protonation of the three secondary amine nitrogen atoms in the macrocycle. The protonation constants of the last amino group and of the pyridine are too low to be detected. The high acidity of the protonated pyridine unit is consistent with the solid-state structure of the perchlorate salt of **L2** which showed only tetraprotonation (on all aliphatic amino groups) of the ligand molecule, despite the very low pH of crystallization. The first two protonation constants of **L2** are both higher than the corresponding values for **L1** resulting in a considerably higher overall basicity of **L2**. Distribution diagrams are shown in the Supporting Information (Figure S2). Table 3 compares the protonation constants of **L1** and **L2** with those reported for analogous, nonpyridine macrocycles. In general, the basicities are lower for the pyridine derivatives, likely caused by the electron-withdrawing effect and/or by the increased rigidity of the macrocycle induced by the pyridine ring. When comparing the basicity of the $N_5$ and $N_3O_2$ macrocycles, the differences originate from the preferential protonation of one of two nonbenzylic amine groups in the pentaaza ligands and/or the generally lower basicity of **L1** due to the electron-withdrawing effect of the highly electronegative oxygen atoms.

Among the metal ions investigated, $Cu^{2+}$ forms the most stable chelates with both **L1** and **L2**. Due to the high affinity of divalent copper for nitrogen donors, the Cu**L2** complex is much more stable than Cu**L1**; it is almost completely formed even at the beginning of the titration (Figure S3, Supporting Information). The stability constants of both ligands follow the Williams−Irving rule: complexes of **L1** show lower selectivity. For **L2**, the stability constant of the $Zn^{2+}$ and $Cd^{2+}$ complexes is about 4 orders of magnitude higher than that of Mn**L2**. Complexes of both ligands form hydroxo-species in alkaline conditions while protonated complexes were detected only with **L2** (Tables 4 and S3, Figures 5 and S4). Hence, the $Mn^{2+}$, $Zn^{2+}$, and $Cd^{2+}$ complexes of **L2** exhibit a stable monoprotonated species with less (e.g., four) donor atoms of the ligand coordinated to the metal ions in acidic solution. For the $Mn^{2+}$ complexes of imine-containing macrocycles,[32] the deprotonation was attributed to ligand changes, most probably to the base-catalyzed water addition to the imine bonds. In our case, the coordinated ligand itself cannot undergo any reaction associated with the consumption or formation of proton(s); therefore, we attribute the deprotonation process to the formation of a hydroxo species. The trends in the stability constants correspond to those found for complexes of 15-ane$N_5$ and 15-ane$N_3O_2$.[53,54] The stability of the $Ca^{2+}$ and $Mg^{2+}$ complexes is remarkably low as compared to the transition metal analogues; thus, the alkaline earth ions should not compete with $Mn^{2+}$ for the ligands under physiological conditions.

As a general conclusion, the replacement of two nitrogens by two oxygen atoms leads to a decrease of the ligand basicity, which is reflected in the lower stability of the $Mn^{2+}$ complex. The complete formation of the Mn**L1** complex is achieved at pH ∼8 while Mn**L2** is fully formed at pH ∼7 (Figure 5).

In order to better compare the stability of the $Mn^{2+}$ complexes, we calculated pMn = $-\log[Mn^{2+}]_{free}$ values corresponding to pH 7.4 and concentrations $c_{Mn} = c_{lig} = 10^{-5}$ M (Table 5). It is evident that the polydentate aminocarboxylates (EDTA, NOTA, DOTA) form much more stable complexes with $Mn^{2+}$ than **L1** and **L2**. Nevertheless, comparing to other 15-membered macrocycles, the introduction of the pyridine ring into the macrocycle leads to an increase of the complex stability.

**Dissociation Kinetics.** The *in vivo* toxicity of $Mn^{2+}$ complexes can be related to the release of free $Mn^{2+}$ *via* proton-catalyzed dissociation or metal-assisted exchange reactions with endogenously available ions such as $Ca^{2+}$, $Cu^{2+}$, or $Zn^{2+}$. In general, even the $Mn^{2+}$ complexes of high thermodynamic stability, like $[Mn(DTPA)]^{3-}$, are kinetically labile. In contrast to $Gd^{3+}$ complexes for which a large body of data has been reported, to the best

**Table 3.** Stepwise Protonation Constants[a] of Various Macrocyclic Ligands (25 °C, $I$ = 0.1 M)

| ligand | log $K_{H1}$ | log $K_{H2}$ | log $K_{H3}$ |
|---|---|---|---|
| **L1**[b] | 8.82 | 7.80 | |
| **L2** | 9.40[b] (9.43,[c] 9.11[d]) | 8.54,[b] (8.80,[c] 8.82[d]) | 5.28[b] (5.28,[c] 5.27[d]) |
| 15-ane$N_3O_2$ | 9.29,[e] 9.51[f] | 8.50,[e] 8.47[f] | 2.12,[e] 2.30[f] |
| 15-ane$N_5$ | 10.31,[c] 10.38,[d] 10.39[g] | 9.29,[c] 9.51,[d] 9.36[g] | 5.93,[c] 5.99,[d] 6.06[g] |

[a] Defined as $K_{Hi} = [H_iL^{i+}]/[H^+] \times [H_{i-1}L^{(i-1)+}]$ for $i$ = 1, 2, 3. [b] This work ($NMe_4Cl$). [c] Ref 25 ($NaClO_4$). [d] Ref 32 ($NaClO_4$). [e] Ref 53 ($NaNO_3$). [f] Ref 54 ($KNO_3$). [g] Ref 55.

**Table 4.** Stability Constants of **L1** and **L2** Complexes with Divalent Metal Ions (25 °C, $I$ = 0.1 M $NMe_4Cl$)

| Constant | $Mg^{2+}$ | $Ca^{2+}$ | $Mn^{2+}$ | $Co^{2+}$ | $Cu^{2+}$ | $Zn^{2+}$ | $Cd^{2+}$ |
|---|---|---|---|---|---|---|---|
| | | | | **L1** | | | |
| log $K_{LM}$[a] | | 2.04 | 7.18 | 9.48 | 13.91 | 8.58 | 8.75 |
| log $K_{LM(OH)}$[b] | | −11.92 | −11.69 | −11.80 | −8.34 | −10.31 | −11.43 |
| log $K_{LM(OH)2}$[b] | | | | | −12.57 | | |
| | | | | **L2** | | | |
| log $K_{LM}$[a] | 3.45 | 2.97 | 10.89 (11.64,[e] 11.12[f]) | d | 21.84 | 16.27 | 15.77 |
| log $K_{HLM}$[c] | | | 4.27 (4.20,[e] 4.51[f]) | d | | 2.45 | 2.70 |
| log $K_{LM(OH)}$[b] | | | −11.52 (−11.54[e]) | d | −12.30 | −11.18 | −11.88 |

[a] $K_{LM} = [LM]/[L] \times [M]$. [b] $K_{LM(OH)i} = [LM(OH)_i(H_2O)_{2-i}] \times [H^+]/[LM(OH)_{i-1}(H_2O)_{3-i}]$ for $i$ = 1, 2. [c] $K_{HLM} = [HLM]/[LM] \times [H^+]$. [d] Oxidation to $Co^{3+}$. [e] Ref 25 ($NaClO_4$). [f] Ref 32 ($NaClO_4$).

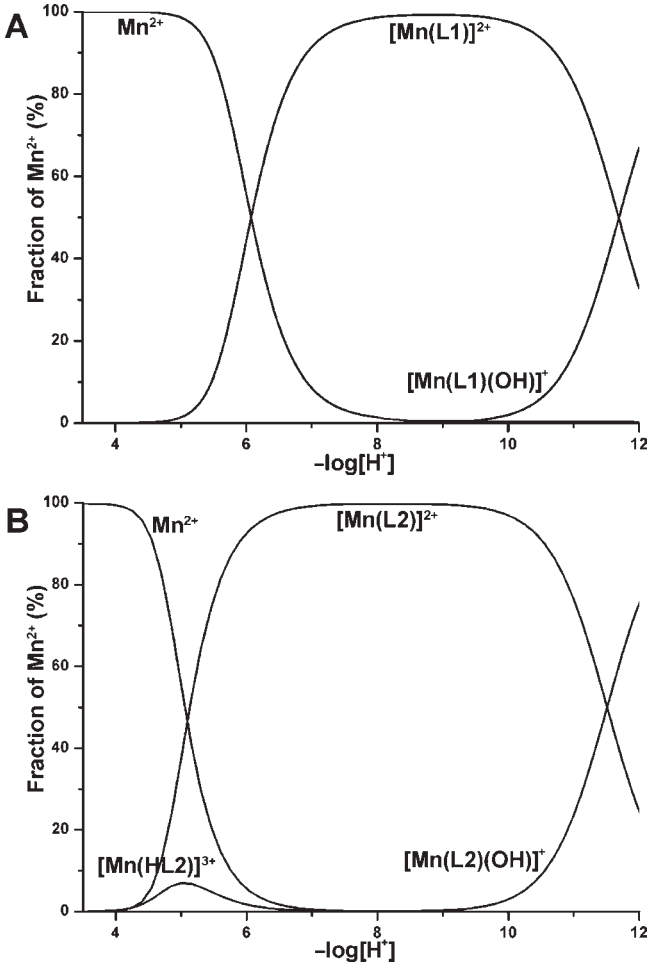


**Figure 5.** Species distribution diagram of the $Mn^{2+}$−**L1** (A) and $Mn^{2+}$−**L2** (B) systems ($c_{Mn} = c_{lig} = 5$ mM, $I = 0.1$ M $NMe_4Cl$, 25 °C).

**Table 5.** pMn Values Calculated for Various $Mn^{2+}$ complexes (pH 7.4, $c_{Mn} = c_{lig} = 10^{-5}$ M)

| ligand | pMn |
|---|---|
| **L1** | 5.28 |
| **L2** | 6.37 (6.60,[a] 6.49[b]) |
| 15-ane$N_3O_2$ | 5.01[c] |
| 15-ane$N_5$ | 5.58,[a] 5.35,[b] 5.44[d] |
| EDTA | 8.01[e] |
| NOTA | 7.94[f] |
| DOTA | 9.09[g] |

[a] Ref 25. [b] Ref 32. [c] Ref 54. [d] Ref 55. [e] Ref [46b]. [f] Ref 56. [g] Ref 23.

of our knowledge, there are no dissociation kinetic studies on $Mn^{2+}$ complexes. In order to describe the kinetic inertness of Mn**L1** and Mn**L2** in a similar way as is commonly done for $Gd^{3+}$ chelates, we investigated the transmetalation reaction with the diamagnetic $Zn^{2+}$ at variable pH through monitoring the release of free $Mn^{2+}$ by relaxometric measurements. The transmetalation of Mn**L1** with $Zn^{2+}$ was too fast to be followed by relaxometry below pH 6. Above pH 6, the partial hydrolysis of

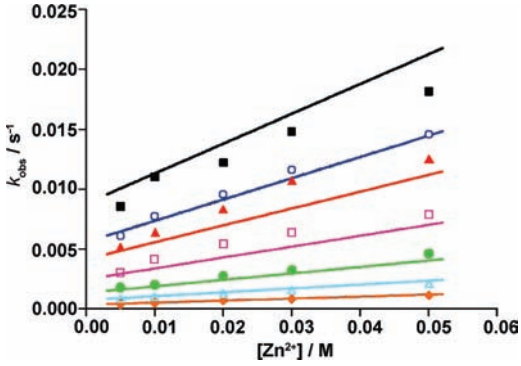


**Figure 6.** Pseudo-first-order rate constants $k_{obs}$ vs $Zn^{2+}$ concentration for the exchange reaction between Mn**L2** and $Zn^{2+}$ ($c_{complex} = 1$ mM, $c_{Zn2+} = 5-50$ mM; pH readings from the bottom are 6.0, 5.7, 5.5, 5.2, 5.0, 4.9, and 4.7). The lines correspond to the best fit with parameters given in Table 6.

$Zn^{2+}$ prevented the measurements. For Mn**L2**, the observed dissociation rate constants in the pH range 4.7−6.0 and in the presence of a 5−50-fold excess of $Zn^{2+}$ are reported in Figure 6 and Table S4 (Supporting Information).

In an excess of the exchanging metal ion, the reaction is of pseudo-first order and the reaction rate is directly proportional to the total concentration of Mn**L2** (eq 1), where $k_{obs}$ is the pseudo-first-order rate constant.

$$-\frac{d[MnL]_{tot}}{dt} = k_{obs}[MnL]_{tot} \quad (1)$$

In general, the dissociation can proceed *via* different pathways, as illustrated in Scheme 2.[57] According to this scheme, the rate of the exchange reaction can be given by eq 2 (in the equations, charges of the complexes are omitted for the sake of clarity).

$$-\frac{d[MnL]_{tot}}{dt} = k_{MnL}[MnL] + k_{MnHL}[MnHL] + {}^{H}k_{MnHL}[MnHL][H^+] + {}^{Zn}k_{MnHL}[MnHL][Zn^{2+}] \quad (2)$$

Here, the first term corresponds to the spontaneous dissociation of the complex (reaction **A** in Scheme 2), the second one to the spontaneous dissociation of the protonated complex (**B**), the third one to the proton-assisted dissociation (**C**), and the last term to the metal-assisted (**D**) dissociation of the protonated complex. The total complex concentration can be expressed as in eq 3:

$$[MnL]_{tot} = [MnL] + [MnHL] \quad (3)$$

The pseudo-first-order rate constant $k_{obs}$ is then defined by eq 4:

$$k_{obs} = \frac{k_0 + k_1[H^+] + k_2[H^+]^2 + k_3[H^+][Zn^{2+}]}{1 + K_{MnHL}[H^+]} \quad (4)$$

where $k_0 = k_{MnL}$, $k_1 = k_{MnHL} \cdot K_{MnHL}$, $k_2 = {}^{H}k_{MnHL} \cdot K_{MnHL}$, and $k_3 = {}^{Zn}k_{MnHL} \cdot K_{MnHL}$.

(53) Hancock, R. D.; Bhavan, R.; Wade, P. W.; Boeyens, J. C. A.; Dobson, S. M. *Inorg. Chem.* **1989**, *28*, 187–194.
(54) Cabral, M. F.; Delgado, R. *Helv. Chim. Acta* **1994**, *77*, 515–524.
(55) Newton, J. E.; Jackels, S. C. *J. Coord. Chem.* **1988**, *19*, 265–277.
(56) Cortes, S.; Brucher, E; Geraldes, C. F. G. C.; Sherry, A. D. *Inorg. Chem.* **1990**, *29*, 5–9.
(57) Sarka, L.; Burai, L.; Brücher, E. *Chem.—Eur. J.* **2000**, *6*, 719–724.

**Scheme 2.** Possible Dissociation Pathways for Mn**L2**

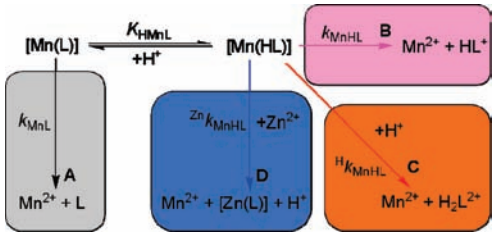


The experimental rate constants were fitted to eq 4, and the calculated parameters are listed in Table 6. The value of the protonation constant of Mn**L2**, $K_{MnHL}$, was fixed to the value obtained from potentiometry (Table 4; when fitting $K_{MnHL}$, we obtained a similar value). During the fitting procedure, $k_0$ had to be set to zero; otherwise the fit gave very small values with large errors. It shows that the spontaneous dissociation of Mn**L2** does not contribute to the overall dissociation. Thus, we can conclude that the dissociation proceeds *via* protonated species involving pathways **B**, **C**, and **D**. Previously, $k_1 = 16\ M^{-1}\ s^{-1}$ has been reported for the dissociation of Mn**L2**.[25] In that study, the $Cu^{2+}$ was used as a ligand scavenger, and the reaction was followed at a single $Cu^{2+}$ concentration (8-fold excess) using UV−vis detection; however, a transmetalation reaction with $Cu^{2+}$ was not considered. Thus, the results could be hardly compared directly.

With the lack of kinetic data available for $Mn^{2+}$ complexes, we compare the rate constants obtained here with those for GdDTPA, a standard $Gd^{3+}$-based MRI contrast agent (GdDTPA = $[Gd(DTPA)(H_2O)]^{2-}$). Overall, the dissociation pathways involving protonated complexes proceed several orders of magnitude faster for Mn**L2** than for GdDTPA. At pH 7.4 and a physiological blood concentration of $Zn^{2+}$ ($10^{-5}$ M),[58] the dissociation of Mn**L2** exclusively occurs *via* spontaneous dissociation of the protonated complex (route **B** in Scheme 2), while under the same conditions, the GdDTPA complex dissociates *via* the direct attack of $Zn^{2+}$ on the complex (compare half-times in Table 6). The direct attack of $Zn^{2+}$ on the Mn**L2** complex at any pH has low probability due to the positive charge of the complex and to the nonavailability of any donor atom for $Zn^{2+}$ binding in the fully $Mn^{2+}$-bound ligand (unlike the negatively charged GdDTPA), and therefore the dissociation *via* a dinuclear complex with $Zn^{2+}$, commonly observed for lanthanide chelates,[57] was not taken into consideration. When this dissociation pathway was included in the fit, we obtained a very small value for the stability constant of the dinuclear complex with large error and an unreliably low rate constant for its dissociation. The dissociation half-life of Mn**L2** at pH 7.4, $c(Zn^{2+}) = 10^{-5}$ M, corresponding to physiological conditions is 11.4 h (Table 6), which means that the complex should stay intact during the course of an MRI experiment (typical elimination times for small-molecular-weight Gd-based agents are a few hours for humans and a few minutes for small animals).

**$^{17}$O NMR and $^{1}$H NMRD Measurements.** In the context of MRI contrast agent research, the efficacy and the paramagnetic relaxation behavior of a paramagnetic chelate is commonly characterized by proton relaxivity measurements as a function of the magnetic field. Such $^{1}$H NMRD profiles are dependent on all microscopic parameters that determine relaxivity, and their shape can often help to distinguish between various relaxation mechanisms. To obtain reliable information on the parameters characterizing water exchange (exchange rate, $k_{ex}$, or residence time, $\tau_M$; $\tau_M = 1/k_{ex}$), rotation ($\tau_R$), and electron spin relaxation, the $^{1}$H NMRD data are usually completed with variable-temperature $^{17}$O NMR measurements. In the $^{17}$O NMR experiment, the longitudinal ($T_1$) and transverse ($T_2$) relaxation times as well as the chemical shifts ($\omega$) of the bulk water are recorded in the presence of the paramagnetic complex. The temperature dependence of $^{17}$O transverse relaxation rates allows for a direct determination of the water exchange rate, $k_{ex}$, whereas the longitudinal relaxation describes the rotational motion of the complex.

**Table 6.** Kinetic Parameters for the Dissociation of Mn**L2** and Comparison to Those for GdDTPA

| constant | Mn**L2** | GdDTPA[a] |
|---|---|---|
| $k_1/M^{-1}\ s^{-1}$ | $423 \pm 31$ | 0.58 |
| $k_2/M^{-2}\ s^{-1}$ | $(1.0 \pm 0.3) \times 10^7$ | $9.7 \times 10^4$ |
| $k_3/M^{-1}\ s^{-1}$ | $(1.7 \pm 0.1) \times 10^4$ | |
| log $K_{MnHL}$ | 4.27[b] | log $K_{HGdL} = 2$ |
| $t_{1/2}$ (pH 6.0, $c(Zn^{2+}) = 10^{-3}$ M) | 26 min | 3.42 h |
| $t_{1/2}$ (pH 6.0, $c(Zn^{2+}) = 10^{-5}$ M) | 27 min | 156 h |
| $t_{1/2}$ (pH 7.4, $c(Zn^{2+}) = 10^{-3}$ M) | 11.0 h | 3.46 h |
| $t_{1/2}$ (pH 7.4, $c(Zn^{2+}) = 10^{-5}$ M) | 11.4 h | 330 h |

[a] Ref 57. [b] Value fixed to that determined by pH potentiometry.

We measured variable-temperature transverse $^{17}$O relaxation times and chemical shifts on aqueous solutions of Mn**L1** and Mn**L2** at pH 8.0 where the complexes are fully formed. The longitudinal relaxation times were also measured; however, they could not be involved in the fitting since they were only slightly (~3−5%) shorter for the solutions containing the $Mn^{2+}$ complexes than those for the diamagnetic reference. The $^{1}$H NMRD profiles were recorded at 25, 37, 50, and 65 °C. The profiles recorded in a TRIS buffer or in PBS were identical. The reduced transverse $^{17}$O relaxation rates and chemical shifts were fitted simultaneously with the $^{1}$H NMRD data according to the Solomon−Bloembergen−Morgan theory of paramagnetic relaxation, as described in the Supporting Information together with the list of fixed parameters during the fitting procedure. The plots of the experimental data for the Mn**L1** and Mn**L2** complexes together with the fitted curves are depicted in Figure 7. The best-fit values of the parameters are shown in Table 7 and compared with data for $[Mn(H_2O)_6]^{2+}$ and other relevant $Mn^{2+}$ chelates. For Mn**L1**, the parameters characterizing the electron spin relaxation are exclusively obtained from the $^{1}$H NMRD data, while for Mn**L2**, they are also determined from the $^{17}$O $1/T_2$ values. For Mn**L2**, the contribution of the electron spin relaxation term ($1/T_{1e}$ in $\tau_{s1}$; eq S4 in Supporting Information) to the transverse relaxation rate varies between 3 and 60%, depending on the temperature. The small contribution of the electron spin relaxation in the fast exchange limit ensures that the value calculated for the water exchange rate is correct.

(58) May, P. M.; Linder, P. W.; Williams, D. R. *J. Chem. Soc., Dalton Trans.* **1977**, 588–595.

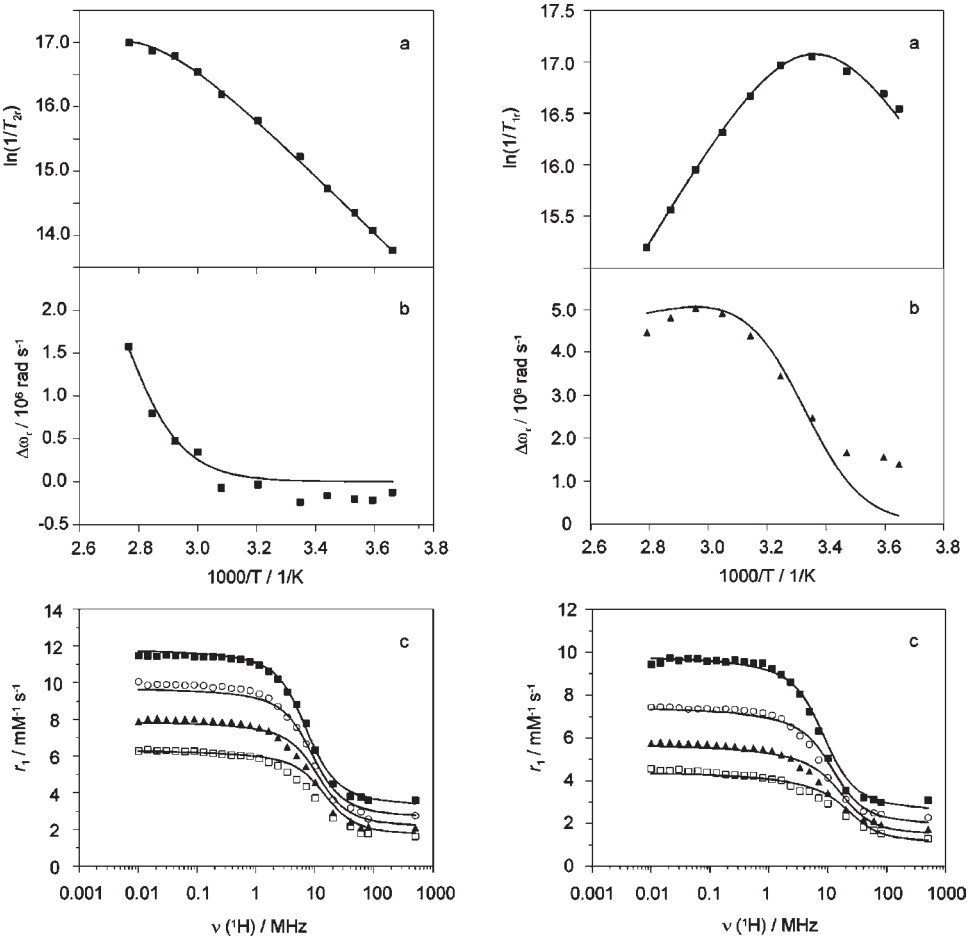


**Figure 7.** Reduced $^{17}O$ transverse relaxation rates (a), chemical shifts (b), and $^{1}H$ NMRD profiles (c) at 25 (■), 37 (●), 50 (▲), and 65 °C (□) measured for $[Mn(\mathbf{L1})(H_2O)_2]^{2+}$ (left) and $[Mn(\mathbf{L2})(H_2O)_2]^{2+}$ (right); $c_{MnL} = 5$ mM, pH 8.0. The full lines represent the results of the best simultaneous fits of $^{17}O$ NMR and $^{1}H$ NMRD data.

**Table 7.** Relaxivity and Best Fit Parameters Obtained from the Simultaneous Analysis of $^{17}O$ NMR and $^{1}H$ NMRD Data for the $[Mn(\mathbf{L1})(H_2O)_2]^{2+}$ and $[Mn(\mathbf{L2})(H_2O)_2]^{2+}$ Complexes

| parameter | $[Mn(\mathbf{L1})(H_2O)_2]^{2+}$ | $[Mn(\mathbf{L2})(H_2O)_2]^{2+}$ | $[Mn_2(ENOTA)(H_2O)_2]$[a] | $[Mn(H_2O)_6]^{2+}$[b] |
|---|---|---|---|---|
| $r_1$ at 25/37 °C (20 MHz)/mM$^{-1}$ s$^{-1}$ | 4.48/3.61 | 3.56/3.13 | 3.39/2.71 | 7.4[c]/− |
| $k_{ex}^{298}/10^7$ s$^{-1}$ | 0.38 ± 0.02 | 6.9 ± 0.7 | 5.5 | 2.1 |
| $\Delta H^{\ddagger}$/kJ mol$^{-1}$ | 35.3 ± 2 | 37.7 ± 4 | 20.5 | 32.9 |
| $\Delta S^{\ddagger}$/J mol$^{-1}$K$^{-1}$ | −1.0 ± 6 | +32 ± 12 | −28 | +5.7 |
| $E_{rH}$/kJ mol$^{-1}$ | 16.1 ± 0.5 | 23.1 ± 0.5 | 18 | |
| $\tau_{rH}^{298}$/ps | 40.3 ± 5 | 28.3 ± 5 | 26 | 30[d] |
| $\tau_v^{298}$/ps | 3.3 ± 0.5 | 3.9 ± 0.2 | 7.7 | 3.3 |
| $\Delta^2/10^{18}$ s$^{-2}$ | 6.6 ± 0.5 | 4.6 ± 0.1 | 4.7 | 5.6 |
| $A_O/\hbar/10^6$ rad s$^{-1}$ | 38.6[e] | 38.6 ± 4 | 32.7 | 33.3 |

[a] ref 22. [b] ref 61. [c] 24 MHz, ref 16. [d] $T = 308$ K, ref 59. [e] Fixed during the fitting procedure.

The shape of the $^{1}H$ NMRD curves is typical of low-molecular-weight compounds. They show only one dispersion between 1 and 10 MHz, as has been observed for other $Mn^{2+}$ complexes,[16,18] with the exception of $[Mn(H_2O)_6]^{2+}$ [59] and $[Mn_2(ENOTA)(H_2O)_2]$,[22] where another dispersion at low field is also observed originating from scalar interactions between the paramagnetic ion and the water proton.

On the basis of the crystal structures and previous results on similar systems,[29−32] the hydration number of both complexes is supposed to be $q = 2$ in aqueous solution. The chloride ion(s) found in the solid-state structure completing the coordination sphere of the manganese(II) is (are) replaced by water molecule(s) in solution. Although chloride has high affinity to $Mn^{2+}$, its substitution by water molecule(s) in diluted aqueous solution was proved by the similar relaxivities of Mn**L2** measured in the presence and absence of chloride ions [$c(Mn^{2+}) = 5$ mM, $c(Cl^-) = 0$ or 250 mM). Likewise, conductivity measurement on analogous complexes also evidenced the replacement of chloride by water.[60]

(59) Bertini, I.; Briganti, F.; Xia, Z.; Luchinat, C. *J. Magn. Reson.* **1993**, Series A *101*, 198−201.
(60) Jackels, S. C.; Durham, M. M.; Newton, J. E.; Henninger, T. C. *Inorg. Chem.* **1992**, *31*, 234–239.

**Table 8.** Comparison of Water Exchange Parameters for Various $Mn^{2+}$ Complexes and for the Aqua Ion (for ligand structures, see Chart 1)

| complex | CN[a] | $k_{ex}^{298}/10^7\ s^{-1}$ | $\Delta H^{\ddagger}$/kJ mol$^{-1}$ | $\Delta S^{\ddagger}$/J mol$^{-1}$ K$^{-1}$ | ref |
|---|---|---|---|---|---|
| $[Mn(\mathbf{L1})(H_2O)_2]^{2+}$ | 7 | 0.38 | 35.3 | −1.1 | this work |
| $[Mn(\mathbf{L2})(H_2O)_2]^{2+}$ | 7 | 6.9 | 37.7 | +32 | this work |
| | | 4.7 | 39.1 | +33 | 32 |
| $[Mn(15\text{-}aneN_5)(H_2O)]^{2+}$ | 6 | ≥10 | | | 32 |
| $[Mn_2(ENOTA)(H_2O)_2]$ | 6 | 5.5 | 20.5 | −28 | 22 |
| $[Mn(EDTA)(H_2O)]^{2-}$ | 7 | 44 | 37.4 | +34 | 66 |
| $[Mn(EDTA-BOM)(H_2O)]^{2-}$ | 7 | 9.3 | 43.1 | +53[b] | 18 |
| $[Mn(EDTA-BOM_2)(H_2O)]^{2-}$ | 7 | 13 | 38.4 | +39[b] | 18 |
| $[Mn(diPh\text{-}EDTA)(H_2O)]^{2-}$ | 7 | 23 | 23−27 | | 17 |
| $[Mn(CyDTA)(H_2O)]^{2-}$ | 7 | 14 | 42.5 | +54 | 19 |
| $[Mn(H_2O)_6]^{2+}$ | 6 | 2.1 | 32.9 | +5.7 | 61 |

[a] CN = coordination number. [b] Calculated from $k_{ex}^{298}$ and $\Delta H^{\ddagger}$.

For Mn**L1**, the reduced $^{17}O$ transverse relaxation rates decrease with decreasing temperature over all the temperature range studied, and only at the highest temperatures does the curve start to turn. It implies that the system is in the slow-exchange regime; hence, the $1/T_{2r}$ values are determined by the water exchange rate. Accordingly, the reduced chemical shifts are close to zero except for the highest temperatures. For Mn**L2**, the reduced transverse relaxation rates and chemical shifts both indicate a fast- and intermediate-exchange regime. The experimental chemical shifts are related to the value of the hyperfine or scalar coupling constant, and they are directly proportional to $q$. By assuming two inner-sphere water molecules, we obtained an $A_O/\hbar$ value which agrees well with those previously reported for $Mn^{2+}$ chelates (~39 MHz); thus it confirms $q = 2$. The scalar coupling constant reported here is a measure of the manganese spin density at the oxygen nucleus. For usual $Mn^{2+}$ complexes, its value is expected to remain in a limited range. For Mn**L1**, the $^{17}O$ hyperfine or scalar coupling constant could not be calculated, as the system is in the slow-exchange limit. In the fit, its value was fixed to that determined for Mn**L2**, which allowed for describing the experimental chemical shifts.

The water exchange rate has been previously reported for various $Mn^{2+}$ complexes as well as for the $[Mn(H_2O)_6]^{2+}$ aqua ion.[61] Several $Mn^{2+}$−enzyme complexes have been investigated, and they showed increased[62] or decreased[63] water labilities as compared to the aqua ion. Among other chelates, such as the complexes of 1,10-phenanthroline,[64] ATP,[65] or the bis(triazamacrocycle) ENOTA,[22] water exchange is only slightly accelerated on complexation, while for the complexes of EDTA[66] and EDTA derivatives,[17−19] it becomes much faster. The water exchange rate calculated for Mn**L1**, $k_{ex}^{298} = 0.38 \times 10^7\ s^{-1}$, is the lowest value reported for a $Mn^{2+}$ complex, while, for Mn**L2**, it is 1 order of magnitude higher, $k_{ex}^{298} = 6.9 \times 10^7\ s^{-1}$, close to the value previously reported.[32] This difference and, in particular, the very low $k_{ex}^{298}$ for Mn**L1** could be related to the formation of hydrogen bonds between the coordinated water molecules and the macrocycle oxygen atoms which do not exist or are weaker between the $H_2O$ and the nitrogen atoms in Mn**L2**. We should note that the two inner-sphere water molecules can be nonequivalent with respect to their water exchange despite the symmetric nature of the complex.

The activation entropy for Mn**L1** is close to zero ($\Delta S^{\ddagger} = -1.1$ J mol$^{-1}$ K$^{-1}$), indicating an interchange mechanism. Since the typical coordination numbers for $Mn^{2+}$ are six or seven, normally six-coordinate complexes present an associatively activated water exchange (e.g., $[Mn(H_2O)_6]^{2+}$, $[Mn_2(ENOTA)(H_2O)_2]$), while seven-coordinate complexes show a dissociatively activated water exchange (e.g., $[Mn(EDTA)(H_2O)]^{2-}$). Dissociatively activated water exchange has been also evidenced for Mn**L2** from previous variable-pressure $^{17}O$ NMR measurements ($\Delta V^{\ddagger} = +3.2$ cm$^3$ mol$^{-1}$, $\Delta S^{\ddagger} = 33$ mol$^{-1}$ K$^{-1}$),[32] and our $\Delta S^{\ddagger} = 32$ mol$^{-1}$ K$^{-1}$ is in good accordance with this (Table 8). The interchange character of the water exchange for Mn**L1** in contrast to Mn**L2** can be likely related to the presence of the two oxygen atoms in the ligand scaffold; otherwise, according to crystallographic data, the very open water-binding site in these planar $Mn^{2+}$ complexes is identical for both Mn**L1** and Mn**L2**. These oxygen atoms in Mn**L1** can participate in hydrogen bonding with surrounding water molecules and facilitate their approach to the inner-coordination sphere before the departure of the leaving water molecule.

We should note that previous EPR measurements on $Mn(15\text{-}aneN_5)$[55,60] confirmed monohydration of the complex (overall coordination number of six), in accordance with $^1H$ NMRD data ($r_1 = 2.3$ mM$^{-1}$ s$^{-1}$, 24 MHz, 25 °C).[55] The relaxivities are about two times higher for $[Mn(\mathbf{L2})(H_2O)_2]^{2+}$, evidencing the presence of two coordinated water molecules. The different coordination numbers nicely reflect the higher rigidity of pyridine-containing ligands **L1** and **L2**, which also leads to higher thermodynamic stability and kinetic inertness of their $Mn^{2+}$ complexes.

**Reaction with Endogenous Anions.** Small endogenous anions like carbonate, phosphate, citrate, etc. are known to interact with coordinatively unsaturated metal complexes by replacing the inner-sphere water molecule(s). The formation of such ternary complexes can be strongly limitative for the *in vivo* relaxivity of the complex, as has been proved for $Gd^{3+}$-DO3A derivatives.[67] In the case of

(61) Ducommun, Y.; Newmann, K. E.; Merbach, A. E. *Inorg. Chem.* **1980**, *19*, 3696–3703.
(62) Reuben, J.; Cohn, M. *J. Biol. Chem.* **1970**, *245*, 6539–6546.
(63) Scrutton, M. C.; Mildvan, A. S. *Biochemistry* **1968**, *7*, 1490–1505.
(64) Grant, M.; Dodgen, H. W.; Hunt, J. P. *Inorg. Chem.* **1971**, *10*, 71–73.
(65) Zetter, M. S.; Dodgen, H. W.; Hunt, J. P. *Biochemistry* **1973**, *4*, 778–782.
(66) Zetter, M. S.; Grant, M.; Wood, E. J.; Dodgen, H. W.; Hunt, J. P. *Inorg. Chem.* **1972**, *11*, 2701–2706.
(67) (a) Aime, S.; Botta, M.; Bruce, J. I.; Mainero, V.; Parker, D.; Terreno, E. *Chem. Commun.* **2001**, 115–116. (b) Bruce, J. I.; Dickins, R. S.; Govenlock, L. J.; Gunnlaugsson, T.; Lopinski, S.; Lowe, M. P.; Parker, D.; Peacock, R. D.; Perry, J. J. B.; Aime, S.; Botta, M. *J. Am. Chem. Soc.* **2000**, *122*, 9674–9684.

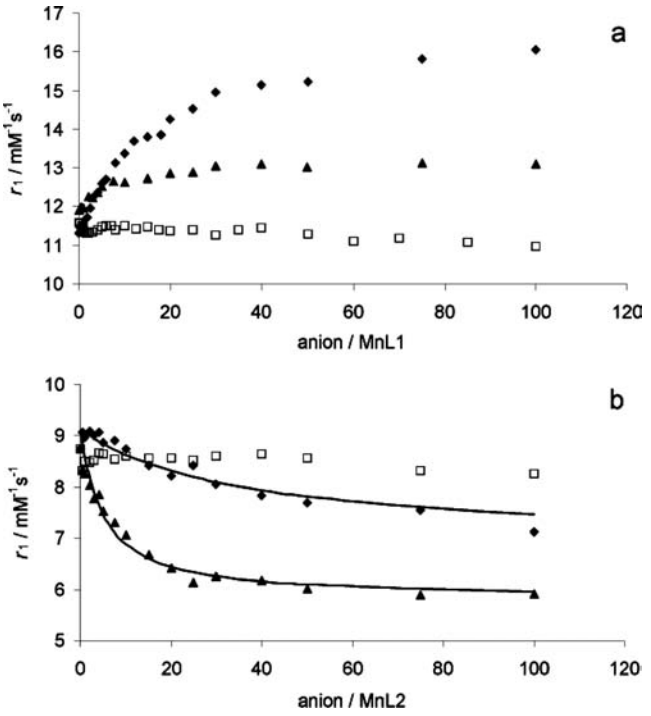


**Figure 8.** $^1$H relaxivities upon the addition of carbonate (□), phosphate (♦), and citrate (▲) to 1 mM Mn**L1** (a) and Mn**L2** (b) (0.1 M TRIS buffer, pH 8.0 at 0.5 MHz, and 25 °C). The full lines represent the results of the fit as explained in the text.

$Gd^{3+}$, ternary complex formation is typically observed for bishydrated chelates, provided the two inner-sphere water molecules occupy adjacent positions. For Mn**L1** and Mn**L2**, the two water molecules are in axial positions on the opposite side of the macrocycle plane, which should be unfavorable for anion binding.

To assess anion binding, proton relaxivities were recorded at 0.5 MHz for Mn**L1** and Mn**L2** solutions in the presence of an increasing amount of phosphate (mixture of $HPO_4^{2-}/H_2PO_4^-$ at pH 8.0), carbonate ($CO_3^{2-}/HCO_3^-$), or citrate ($cit^{3-}/Hcit^{2-}$; Figure 8). Carbonate has no effect on either of the complexes. For Mn**L1**, the relaxivities increase upon the addition of phosphate or citrate. The most evident reasons could be the release of free $Mn^{2+}$ or aggregate formation. The decomposition of the complex and release of free $Mn^{2+}$ could be promoted by an interaction between the free ligand and phosphate (or citrate), as some polyazamacrocycles behave as efficient receptors of phosphate.[68] This hypothesis was excluded by the identical NMR spectra of the ligand in the presence and in the absence of phosphate (pH 2−12). In addition, on the basis of the stability constants,[46] phosphate and citrate cannot replace **L1** in Mn**L1**. We have also recorded the $^1$H NMRD profile of Mn**L1** in the presence of 100 equiv of phosphate, which showed increased relaxivity all over the measured magnetic field range (see Figure S5, Supporting Information) without the low-field dispersion typical of free $Mn^{2+}$. The $^1$H NMRD profile does not show the typical high field peak characteristic of slowly tumbling aggregates either, excluding therefore the formation of large aggregates. One plausible explanation for the small relaxivity increase upon the addition of phosphate or citrate could be the formation of anion-bridged dimers/small oligomers with an important second sphere relaxivity effect (with possible prototropic exchange on the bound and protonated phosphate ions).

In the case of Mn**L2**, the relaxivities decrease when increasing amounts of phosphate or citrate are added, in agreement with the replacement of an inner-sphere water molecule by the anion. The plots of the relaxivity versus the [anion]/[complex] ratio show saturation profiles for these two anions. The least-squares fitting of the titration profiles allowed us to estimate the binding constants, $K = 20 \pm 5\ M^{-1}$ for phosphate and $K = 100 \pm 7\ M^{-1}$ for citrate. These constants indicate a relatively weak binding of the anions (despite the positive charge of the complex), which can be related to the fact that they can only bind in a monodentate manner since these two inner-sphere water molecules are not adjacent. These anion interactions are weaker than those for complexes of DO3A derivatives. The relaxivity of each ternary complex, as obtained in the fit, is $r_{1,t} = 5.8 \pm 0.2\ mM^{-1}\ s^{-1}$, which is consistent with the replacement of only one inner-sphere water molecule.

**Electrochemistry.** The oxidation of $Mn^{2+}$ to $Mn^{3+}$ resulting in a lower spin can strongly influence the relaxivity of the complex. Thus, cyclic voltammograms of Mn**L1** ($E_{ox} = 1.11$ V and $E_{red} = 0.94$ V vs NHE) and Mn**L2** ($E_{ox} = 1.24$ and $E_{red} = 1.01$ vs NHE) were measured, and both exhibit a quasi-reversible $Mn^{III}L/Mn^{II}L$ couple with relatively high formal redox potentials (for the experimental conditions and the cyclic voltammograms, see the Supporting Information (Figures S6 and S7)). Our results correspond well to the data published previously for Mn**L2** in anhydrous MeOH ($E_{1/2}$ ~0.8 V)[25] and for $[Mn(Me_2\text{-}15\text{-}pyaneN_5)]^{2+}$ in an aqueous HEPES buffer (HEPES = 4-(2-hydroxyethyl)-1-piperazineethanesulfonic acid).[30] The values obtained are slightly higher than those for the $[Mn(NOTA)]^-$ and $[Mn(EDTA)(H_2O)]^{2-}$ complexes[69] and indicate a good stabilization of the divalent manganese in complexes with macrocycles **L1** and **L2**. The formal redox potentials show that both Mn**L1** and Mn**L2** complexes have a low tendency to be oxidized by air oxygen. This confirms their stability toward oxidation under the experimental conditions used in the kinetic and NMR studies.

## Conclusions

Two pyridine-based macrocycles, **L1** and **L2**, were prepared and characterized. Potentiometry was used to determine the protonation constants of both ligands as well as the stability constants of metal complexes formed with $Mn^{2+}$, endogenously important ($Ca^{2+}$, $Cu^{2+}$, $Zn^{2+}$), and some other metal ions ($Co^{2+}$, $Cd^{2+}$, $Mg^{2+}$). The incorporation of the pyridine into the macrocyclic scaffold increases the rigidity of the complexes and leads to a greater thermodynamic stability. The substitution of oxygen with nitrogen in the macrocycle results in a higher ligand basicity and, consequently, an increased stability of the complexes. The solid-state structures of Mn**L1** and Mn**L2** confirm the coordination number of 7 for $Mn^{2+}$ and the presence of $Cl^-$ and $H_2O$ in axial

(68) Develay, S.; Tripier, R.; Le Baccon, M.; Patinec, V.; Serratrice, G.; Handel, H. *Dalton Trans.* **2005**, 3016–3024.

(69) Fukuda, Y.; Hirota, M.; Kon-no, M.; Nakao, A.; Umezawa, K. *Inorg. Chim. Acta* **2002**, *339*, 322–326.

positions. Electrochemical measurements yielded a formal redox potential of ~1 V, which confirms the resistance of the divalent manganese in the complexes toward air-oxidation. $^{17}O$ NMR and $^{1}H$ NMRD measurements were performed on Mn**L1** and Mn**L2** to determine the microscopic parameters governing their relaxivity. The water exchange rate for Mn**L1**, $k_{ex}^{298} = 0.38 \times 10^7\ s^{-1}$, is the lowest value ever measured for a $Mn^{2+}$ complex and is about 20-times lower than $k_{ex}^{298} = 6.89 \times 10^7\ s^{-1}$ on the Mn**L2** complex. Our results indicate that water exchange is highly sensitive even to minor changes in the ligand structure, similarly to $Gd^{3+}$ complexes. Water exchange on Mn**L2** is fast enough to achieve high relaxivity upon conjugation of the complex to slowly tumbling, large molecules. The proton/zinc(II)-catalyzed dissociation of Mn**L1** is too fast to be studied by conventional relaxivity measurements under pH 6. For Mn**L2**, the prime importance of the proton-assisted dissociation was evidenced; the $Zn^{2+}$ catalysis is not important at physiological pH. Relaxometric anion-binding studies revealed weak interactions between Mn**L2** and phosphate or citrate, leading to the formation of monohydrated species. Mn**L1** seems to form oligomeric species in the presence of phosphate, resulting in an increased relaxivity. Carbonate shows no interaction with either of the complexes.

The inclusion of the pyridine in the macrocycle scaffold induces crucial changes in several aspects. Most importantly, it increases the thermodynamic and the kinetic stability of the $Mn^{2+}$ complexes. The presence of the pyridine rigidifies the ligand backbone, which leads to different coordination numbers of the $Mn^{2+}$ complexes (CN 7 for **L2** with respect to 6 for 15-ane$N_5$).

The relaxivity of the studied complexes is higher than those of typical low-molecular-weight $Gd^{3+}$ chelates. In general, the toxicity of manganese is much lower with respect to that of gadolinium; moreover, the kinetic inertness of these macrocyclic $Mn^{2+}$ chelates can likely be further improved by rigidifying the macrocycle backbone.

The complexes presented here and their derivatives are known to be excellent SOD mimics, nearing the efficacy of the enzyme itself. Considering the concentrations that would be needed *in vivo* for successful contrast enhancement, the SOD activity would likely prevent any in vivo imaging application. Nevertheless, the results obtained on these model compounds give insight into the relaxation behavior of $Mn^{2+}$ complexes in general with respect to MRI contrast agent applications.

**Acknowledgment.** We thank Ms. M. Malíková, Dr. J. Havlíčková, and Dr. V. Kubíček for their help with the titration experiments. Support from the Grant Agency of the Academy of Science of the Czech Republic (No. KAN201110651) and the Long-Term Research Plan of the Ministry of Education of the Czech Republic (No. MSM0021620857) is acknowledged. B.D. acknowledges the Ph.D. grant of the RFR program of the French Ministry of Education and Research. The work was carried out in the frame of COST D38 (MŠMT OC 179) and the EU-supported NoE projects (6th FP) DiMI (No. LSHB-2005−512146) and EMIL (LSCH-2004-503569). Dr. I. Císařová is acknowledged for acquiring the RTG diffraction data and Prof. J. Barek for providing electrochemical equipment.

**Supporting Information Available:** Synthesis and characterization of precursors and **L2**; selected crystallographic data for [Mn(**L1**)($H_2O$)Cl]($ClO_4$)·$H_2O$, [Mn(**L1**)$(Cl)_2$][Mn(**L1**)($H_2O$)-Cl]Cl·1.5$H_2O$, and [Mn(**L2**)$(Cl)_2$]-[Mn(**L2**)($H_2O$)Cl]$_2Cl_2$·4$H_2O$; overall protonation/stability constants of **L1** and **L2** and their complexes with divalent metal ions as well as species distribution diagrams for **L1**, **L2**, and their systems with $Cu^{2+}$ and $Zn^{2+}$; observed pseudo first-order rate constants $k_{obs}$ for dissociation of Mn**L2**; $^{1}H$ NMRD profile of Mn**L1** in the absence and in the presence of 100 mol equiv of phosphate; conditions of cyclic voltammetry; voltammograms of Mn**L1** and Mn**L2**; and equations used for the analysis of the $^{17}O$ NMR and $^{1}H$ relaxivity data together with the parameters fixed during the fitting procedure. This material is available free of charge via the Internet at http://pubs.acs.org.